Applied Catalysis B: Environmental 321 (2023) 122064

Contents lists available at ScienceDirect

Applied Catalysis B: Environmental

journal homepage: www.elsevier.com/locate/apcatb

Intermetallic PdZn/TiO_2 catalysts for methanol production from CO_2 hydrogenation: The effect of ZnO loading on PdZn-ZnO sites and its influence on activity

Carlos Quilis, Noelia Mota, Barbara Pawelec, Elena Millán, Rufino M. Navarro Yerga *

Grupo de Energía y Química Sostenibles, Instituto de Catálisis y Petroleoquímica, CSIC, Marie Curie 2, 28049 Madrid, Spain

ARTICLE INFO

Keywords:
Methanol synthesis
CO_2 hydrogenation
PdZn, intermetallic, ZnO, TiO_2

ABSTRACT

In this work, intermetallic PdZn-ZnO catalysts supported on high surface area TiO_2 were synthesized using metal-organic precursors and different Zn/Pd molar ratio (2.5, 5 and 7.5). The use of organic Pd and Zn precursors in the impregnation of TiO_2 has made it possible to achieve the formation of PdO and ZnO nanoparticles that facilitate the uniform formation of small intermetallic β-PdZn particles after reduction with hydrogen at 450 °C. No significant differences in formation, crystallinity or size of intermetallic PdZn particles with varying the Zn concentration were observed. The differences were in the characteristics of the ZnO particles that lead to enhanced development of the contacts between the PdZn and ZnO particles . The best methanol yield (78.9 $mmol_{MeOH} \cdot min^{-1} \cdot mol_{Pd}^{-1}$) was obtained over the catalyst with highest ZnO content. This was consequence of the higher development of PdZn-ZnO interfaces, where CO_2 adsorption and hydrogenation of intermediate species to methanol occurs, as well as of the higher stability of the largest ZnO particles under reaction conditions.

1. Introduction

Methanol is one of the most widely produced compounds in the chemical industry because of its importance as a primary chemical product for the synthesis of plastics, resins, paints, etc. [1]. In addition, methanol is considered as alternative fuel due to its high energy density and the possibility of being synthesized from renewable resources. This versatility led to the first appearance in 2005 of the term "methanol economy" proposed by Olah [2]. Although there are several methods for methanol production, the most recently investigated is its direct production by catalytic hydrogenation of CO_2 (Eq. 1), due to the interest in reducing global CO_2 emissions with the additional advantage of being an indirect method for the chemical storage of renewable hydrogen [2].

$$CO_2 + 3\ H_2 \rightleftharpoons CH_3OH + H_2O\ \Delta H_{298\ K} = -49{\cdot}5\ kJ\ mol^{-1} \quad (1)$$

Despite the great interest in the catalytic hydrogenation of CO_2 to methanol, there are still certain limitations associated with its slow kinetics and low conversion that require the selection and development of active catalysts compatible with the thermodynamic operating conditions favorable for the production of methanol (low temperature and high pressure) [3,4]. The well-known Cu/Zn-based catalysts are very efficient and stable systems for the selective production of methanol from syngas (mixture of CO and H_2) and are also the most studied catalysts for the hydrogenation of CO_2 to methanol [1–4]. However, these catalysts are prone to deactivation [5] and their efficiency is significantly reduced when pure CO_2 is used instead of syngas [6–8] due to their excessive surface oxidation, segregation and sintering of the active Cu/Zn sites by the excess of water produced in the hydrogenation of CO_2 to methanol [4,9].

Despite the efforts made to improve the activity and stability of Cu/Zn catalysts applied to methanol synthesis from CO_2, excessive deactivation and poor selectivity to methanol due to the reverse water gas shift reaction (RWGS) remain major obstacles restricting their application. To overcome the selectivity and stability limitations of conventional Cu/Zn-based catalysts, alternative copper-free catalysts based on palladium, gallium intermetallic compounds, In_2O_3, etc. have been investigated to develop more active and stable formulations for methanol synthesis from CO_2 [10–12]. Among the alternative formulations developed, those based on Pd as the active phase are the second most studied due to their high activity, stability and selectivity to methanol. Within the Pd-based catalysts, PdZn intermetallic compounds proved to be promising and their efficiency and high selectivity were demonstrated in the hydrogenation of CO_2 to methanol [13–32] as well as in

* Corresponding author.
E-mail address: r.navarro@icp.csic.es (R.M. Navarro Yerga).

https://doi.org/10.1016/j.apcatb.2022.122064
Received 29 July 2022; Received in revised form 2 October 2022; Accepted 6 October 2022
Available online 8 October 2022

other reactions such as steam reforming of methanol [33–39], CO oxidation [40,41], oxidation of alcohols [41] or selective hydrogenations [42–44]. In fact, PdZn intermetallic catalysts proved to be more efficient for methanol synthesis from CO_2 than other PdIn and PdGa intermetallic systems also claimed as high active methanol synthesis catalysts [14]. Although the intermetallic compound PdZn is known to be the active phase in this reaction, its activity depends on its dispersion, size [45] and/or its close contacts with the ZnO particles [46].

The control of the formation and composition of PdZn intermetallic nanoparticles is necessary because the binary phase diagram of PdZn comprises several compositions. However, the intermetallic β-PdZn (1:1) compound is the phase mainly formed when using classical catalysts preparation methods, such as impregnation or coprecipitation, with subsequent reduction with hydrogen or other reducing gases at elevated temperature (>400 ºC) [40]. In addition to the β-PdZn phase, formation of the α-PdZn phase was also reported when Zn is present at a low concentration on the Pd (111) surface [41]. The most commonly used method for preparing supported PdZn intermetallic compounds is the impregnation of ZnO with palladium precursors. In this method, the formation of PdZn intermetallic particles by heating in hydrogen at high temperature is based on the reduction of ZnO, assisted by H_2-spillover on Pd metallic particles, followed by the Zn diffusion into the Pd nanoparticles [38]. Diffusion of metallic Zn toward the Pd planes and/or the defect sites leading to the formation of a thermodynamically stable β-PdZn intermetallic compound ($\Delta H = -100.4$ kJ mol^{-1}) is possible because of the smaller size of the zinc atoms with respect to palladium atoms (0.135 Å vs. 0.140 Å) [37,40]. This mechanism of PdZn formation by reduction results in PdZn particles in contact with the ZnO particles [46]. However, in the case of Pd and ZnO of small particle size, the diffusion of Zn into the Pd particles could stop the dissociative adsorption of hydrogen on Pd, and, in turn, stop the reduction of ZnO. In this regard, the work by De Waele et al. [47] suggest that simple reduction of small particles of Pd and ZnO generated from hydrotalcite leads to the formation of core-shell particles having a PdZn in the shell and Pd in the core.

For the selective production of methanol via CO_2 hydrogenation, the importance of the formation of the intermetallic compound β-PdZn [18] and the presence of ZnO in the near-surface region of PdZn particles has been highlighted [19]. The complete formation of the intermetallic β-PdZn compound from Pd and ZnO particles is crucial for the selective methanol production because metallic Pd mainly produce CO through the reverse water-gas shift (RWGS) reaction [25,48]. A variety of Pd/ZnO catalysts prepared by different techniques were investigated for CO_2 hydrogenation [18] and a linear relationship between methanol selectivity and CO_2 conversion was observed for all of Pd/ZnO catalysts indicating that the catalytic performance was determined by the presence of the intermetallic compound β-PdZn. The different selectivity of PdZn with respect to Pd was explained by the formation of heteroatomic bonds in the intermetallic compound PdZn, by electron transfer from Zn to Pd, which changes the electronic environment in the intermetallic compound with respect to pure Pd.

A mechanistic study comparing model catalysts Pd(111) and PdZn (111) for CO_2 hydrogenation has shown that the strong electron-donor character of PdZn compared to Pd weakens the adsorption of carbon-bound species and enhances the binding of oxygen-bound species. As a consequence, CO_2 hydrogenation produces as first step formate or carbonate intermediates on PdZn that hydrogenates to methanol, whereas carboxyl intermediates are formed on Pd that produce CO via RWGS [32]. In addition to the formation of the PdZn alloy, its contacts with ZnO are crucial for the selective production of methanol, since in the absence of contacts with ZnO, the intermetallic compound PdZn tends to produce CO, while the intimate contact of the intermetallic compound with ZnO significantly increases the selective production of methanol [19]. It is believed that the contact between PdZn and ZnO stabilizes the intermediate formate or carbonate species following a bifunctional mechanism with CO_2 activation on the ZnO and, H_2 dissociation followed by hydrogen spillover onto PdZn nanoparticles, respectively, to reduce the formate species to methanol [14,30].

Considering that the formation of intermetallic PdZn compound occurs at the interfaces between Pd metal and partially reduced ZnO_x species, the dispersion of PdZn in contact with ZnO is a critical factor influencing on the number of active sites formed. In this regard, the nature of the support is of great importance because it influences the size and site interactions of the PdZn-ZnO interfaces. However, the use of supports to obtain highly dispersed PdZn-ZnO catalysts is a challenging task, and several supports (TiO_2, CeO_2, ZrO_2, Al_2O_3, etc.) have been studied to improve the PdZn-ZnO contacts and surface exposition [3,24,38]. Among the different types of materials that have been tested as supports for PdZn-ZnO, Bahruji et al. [27] demonstrated that TiO_2 was a support that allowed highly dispersed PdZn particles with a small average diameter, resulting in superior methanol productivity. Within this scenario, in this work we investigate the effectiveness of a high surface area TiO_2 (anatase) to disperse and stabilize PdZn-ZnO active species. To disperse the PdZn-ZnO species on the TiO_2 support, it should be noted that the formation of intermetallic PdZn proceeds at interfaces between Pd metal and partially reduced ZnO_x species. Thus, to obtain uniform PdZn particles it is necessary that the structure and size of the Pd and ZnO particles are homogeneous which requires optimization of the preparation method. The formation of PdZn intermetallic compounds and the inhibition of the formation of elemental palladium or Zn-poor intermetallic compounds or alloys, are highly dependent on the catalyst preparation method, Pd precursors, Pd/Zn ratio, reduction temperature, etc. Considering the catalyst preparation method, it has been shown that the use of inorganic Pd and Zn precursors for support impregnation leads to the formation of non-uniform deposits of Pd and ZnO particles that negatively affect the formation of uniform PdZn intermetallic compounds [14]. Compared to these precursors, the use of organic Pd and Zn precursors led to the formation of low-sized and uniform PdZn intermetallic particles [18], although studies using these precursors are scarce. The formation of PdZn intermetallic particles is also highly dependent on the reduction temperature, as described for the PdZn/ZnO catalysts supported on $ZnFe_2O_4$ [24] and Al_2O_3 [38]. In these studies, it was shown that the formation of the β-PdZn phase takes place at 200–400 °C while at higher temperature a Zn-rich alloy is formed [14]. The study of the effect of Pd:Zn ratio on the formation of PdZn intermetallic compounds supported on CeO_2 by Ojelade et al. [3] suggested that the formation of the β-PdZn phase could be maximized using a Pd:Zn molar ratio close to 1. Similarly, for PdZn catalysts supported ZnO-enriched $ZnFe_2O_4$ spinel oxides, Wang et al. [24] observed a volcano curve trend for both CO_2 conversion and methanol selectivity with the Pd/Zn ratio, implying the importance of adequate ZnO content for PdZn intermetallic formation. Therefore, the Pd/Zn ratio in supported PdZn-ZnO catalysts is a key parameter because this ratio determines the formation and contacts of the intermetallic PdZn and ZnO particles on the support. In previous investigations, stronger interaction and easier formation of the intermetallic PdZn was found when Pd was in contact with the more polar facets of ZnO [49].

In this work we present a systematic study of the effectiveness of the use of a high surface area TiO_2 (anatase) support to disperse and stabilize the active PdZn-ZnO species. Supported PdZn-ZnO/TiO_2 catalysts have been prepared using organic metal precursors to obtain Pd and ZnO particles homogeneous in structure and size. To further investigate the role of the formation of PdZn and its contacts with ZnO on the control of activity and selectivity, the effect of the Zn/Pd ratio was systematically studied in the supported catalysts. Previous studies in the literature on the application of PdZn/ZnO catalysts to the synthesis of methanol from CO_2 are scarce, and we consider that the results of this work add some insight into the role of the Zn/Pd ratio in the formation of contacts between supported PdZn and ZnO that directly affect methanol production and catalyst stability under reaction. The activity of the catalysts were evaluated in the selective production of methanol via CO_2 hydrogenation under mild reaction conditions (250 °C, 30 bar) and the activity-

structure correlations of the catalyst has been discussed taking into account its deep characterization by several techniques, such as N_2 physisorption, ICP-OES, Raman spectroscopy, in situ XRD, H_2-TPR, HRTEM, CO-DRIFT and TPD of adsorbed H_2.

2. Experimental

2.1. Catalysts preparation

A series of TiO_2-supported PdZn catalysts were prepared in which the palladium concentration was kept constant (4% by weight) and the amount of Zn was varied to obtain nominal Zn/Pd atomic ratios of 2.5, 5 and 7.5 (Table 1). A high area TiO_2 (100% anatase, 99%, Alfa Aesar) was used as a support to improve the dispersion and surface exposure of the PdZn-ZnO species. Prior to synthesis, the support was ground and sieved to a size between 0.212 and 0.425 mm and it was then calcined under static air at 500 °C for 4 h with a heating ramp of 2 °C/min.

To avoid the use of inorganic precursors that have a negative effect on the dispersion of Pd and Zn, organic precursors of palladium (acetylacetonate, 99%, Sigma-Aldrich) and zinc (acetylacetonate, 100%, Sigma-Aldrich) were used as precursors. Solutions of Pd and Zn acetylacetonate were prepared using chloroform and methanol as solvents, respectively. The incorporation of the Pd and Zn precursors on the TiO_2 support was carried out by the sequential wet impregnation method, incorporating Zn first. The impregnation was performed at room temperature under inert atmosphere using a rotary evaporator (BÜCHI RE-111-Water Bath). In a flask, the support and the volume of zinc precursor solution were added and stirring was maintained for 30 min. Subsequently, the solvent was evaporated at 40 °C under vacuum. Next, the palladium salt solution was added using the same procedure in the rotary evaporator. Finally, the samples were calcined under static air at 350 °C for 2 h with a ramp of 2 °C/min to remove the organic groups from the acetylacetonate and fix the ZnO and PdO particles on the TiO_2 support. The synthesized catalysts are denoted hereafter as PdZn/Ti-*x*, where *x* is the corresponding Zn/Pd atomic ratio (2.5, 5 and 7.5).

A reference catalyst based on Pd supported on TiO_2 (Pd/Ti) was additionally prepared with the same palladium concentration and following the same methodology previously described for the PdZn catalysts to highlight the importance of the presence of Pd and ZnO on the activity and selectivity of the catalysts.

2.2. Catalysts characterization

2.2.1. Chemical analysis

The experimental composition of the elements present in calcined PdZn/Ti catalysts was determined by inductively coupled plasma atomic emission spectroscopy with optical detection (ICP-OES) carried out with a Perkin Elmer Optima 3300DV apparatus. The solid samples were digested with a mixture of HF, HCl, and HNO_3 acids in a microwave oven for 2 h. Then, aliquots of solution were diluted to 50 mL using deionized water (18.2 mΩ quality).

Table 1
Chemical composition (ICP-AES) and mean crystallite size (TiO_2, ZnO from XRD) for calcined PdZn/Ti catalysts.

	ICP-OES			Crystallite size (XRD)	
	Pd (wt %)	Zn (wt %)	Zn/Pd molar ratio	TiO_2 (nm)	ZnO (nm)
PdZn/Ti-2.5	3.5	6.1	2.8	17.9	11.9
PdZn/Ti-5	3.7	12.3	5.4	17.9	13.2
PdZn/Ti-7.5	3.8	19.0	8.1	17.8	14.4

2.2.2. X-ray diffraction (XRD)

Crystalline phases in calcined and reduced PdZn/Ti catalysts were determined with a Polycrystal X'Pert Pro PANalytical computerized diffractometer using Cu Kα radiation (λ = 0.15406 nm). The acquired X-ray diffraction (XRD) patterns covered an angular range between 4 ° and 90 °. The XRD patterns were recorded with a step size of 0.0335 ° and step acquisition time of 200 s. The assignment of the different crystalline phases was based on Joint Committee on Powder Diffraction Standards (JCPDS) powder diffraction cards. In order to analyze the temperature, range in which the PdZn intermetallic compound is formed, calcined $PdZn/TiO_2$ catalysts were studied by in situ XRD under 10% H_2/Ar flow from room temperature, increasing each 50 ºC, until 450 ºC (1 h) with a heating rate of 5 ºC/min. The XRD profiles were collected each 50 ºC using the same parameters described previously.

2.2.3. Raman microscopy

Raman spectra of calcined PdZn/Ti catalysts were acquired using a *RENISHAW inVia* Raman microscope, equipped with a *Leica* microscope, a CCD detector cooled at − 70 ºC, *super-Notch* holographic filters to remove elastic dispersion, a 532 nm diode excitation source (and 325 nm for UV measurements) with a maximum power of 100 mW and an 1800 lines/mm grating monochromator. The spectra were collected using static mode (at 965 cm^{-1}), accumulations of 20 s and spectral resolution of 1 cm^{-1} with a lens of 50x.

2.2.4. N_2 adsorption-desorption isotherms

The porous textural structure of pristine TiO_2 support and calcined PdZn/Ti catalysts were determined by means of N_2 physisorption at − 196 ºC in a Micromeritics-TriStar 3000 apparatus. Prior to N_2 physisorption measurements, samples were degassed in vacuum at 120 ºC for 16 h. The specific surface area was estimated by applying the BET method for adsorption data in the region of 0.05–0.3 relative pressures. Adsorption data were also taken to estimate the cumulative pore volume at $P/P_0 \sim 0.99$ and pore size distributions (PSD) were determined using the Barrett-Joyner-Halenda (BJH) model for mesopores (2.0 nm < pore width < 50.0 nm) [50].

2.2.5. H_2-Temperature programmed reduction (H_2-TPR)

The reducibility of Zn and Pd oxides and the conditions to be applied for the reduction of calcined PdZn/Ti catalysts to obtain the intermetallic PdZn compound were determined from temperature programmed reduction tests with hydrogen.

The measurements were carried out on a Micromeritics TPD/TPR 2900 instrument equipped with a thermal conductivity detector (TCD). Prior to analysis, the sample (0.05 g) was pre-treated with He flowing at a rate of 30 mL(N)·min^{-1} at 120 °C for 20 min to clean the sample and remove physisorbed water. The sample was then cooled in He and the temperature was reduced below ambient (−65 ºC) by immersing the reactor in a vessel with isopropanol and liquid nitrogen. Subsequently, the sample was placed in contact with a gaseous H_2/Ar mixture (10% vol. H_2) at a flow rate of 50 mL(N)·min^{-1} and subjected to a programmed temperature increase at a rate of 5 °C·min^{-1} until 450 °C was reached, which temperature was maintained for 1 h.

2.2.6. H_2-Temperature programmed desorption (H_2-TPD)

The hydrogen adsorption capacity of the freshly reduced PdZn/Ti catalysts was measured on the same Micromeritics TPD/TPR 2900 instrument used for H_2-TPR characterization. Prior to hydrogen adsorption, the sample (0.1 g) was reduced at 450 °C for 1 h (heating rate of 5 °C/min) under a 10% vol. H_2/Ar gas mixture flow (50 mL(N)·min^{-1} total flow). After reduction, the catalyst was purged at the same temperature under an argon flow (50 mL(N)·min^{-1}) for 0.5 h and then cooled to room temperature. H_2 adsorption was performed at room temperature for 1 h using a 10% vol. H_2/Ar mixture (50 mL(N) min^{-1} total flow), followed by purging the catalyst with Ar flow (50 mL(N)·min^{-1}) at the same temperature for 1 h. Finally, programmed desorption

of adsorbed hydrogen experiments was performed by heating the sample from room temperature to 450 °C (10 °C·min^{-1}) under Ar flow (50 mL (N)·min^{-1}).

2.2.7. CO-DRIFTS

The evolution of the active phases with reduction temperature was studied by DRIFT spectroscopy using the CO model molecule on a JASCO FT/IR-6300 spectrometer equipped with a MCT detector cooled by liquid nitrogen. The experimental procedure was as follows. First, the calcined catalysts diluted with KBr (20% by weight) were pre-treated with flowing air (40 mL(N)·min^{-1}) at 350 °C for 20 min (heating rate of 5 ºC min^{-1}) and purged with He flow to cool to room temperature. Then, the sample was reduced with a 10% vol. H_2/He gas mixture at different temperatures (70–250–350–400–450 °C) for 10 min (flow rate of 4 mL(N)·min^{-1}). After this step, H_2 was removed from the DRIFT cell by purging with He for 10 min. Next, CO chemisorption was performed at 25 °C for 20 min using a 5% vol. CO/Ar gas mixture. The spectra were recorded with a resolution of 4 cm^{-1} using 300 accumulations.

2.2.8. High-resolution transmission electron microscopy (HRTEM)

The morphology and particle size distribution of PdZn/Ti catalysts reduced at 450 °C were studied by high-resolution JOEL JEM- 2100 F transmission electron microscope operating at 200 kV with a structural resolution of 0.14 nm. Fresh reduced PdZn/Ti samples preserved in isooctane were crushed and ultrasonically dispersed at room temperature. Next, drop of this solution was deposited on a holey, amorphous carbon-coated Cu TEM grid. The particle size distribution was obtained by statistical treatment of a minimum 200 particles using the equation $d = \sum n_i \cdot d_i / \sum n_i$, where n_i is the number of particles with diameter d_i and $\sum n_i$ is the number of particles. The local elemental analysis of the selected zones carried out to by an energy dispersive X-ray analysis (EDS) method using EDAX spectrometer. Fast Fourier Transformation (FFT) and Inverse fast Fourier Transformation (IFFT) were used to index the lattice spacing of specific crystals.

2.3. Catalytic activity measurements

The catalyst activity measurements were carried out in an experimental unit consisting of a feed system, a reaction system and a reaction product analysis system. The feed system consists of several gas lines, each with a pressure reducer, a particulate filter, a flow controller and indicator, and a non-return valve. The reaction system consists of a fixed-bed tubular reactor made of stainless steel, with an internal diameter of 0.8 cm and a length of 22.4 cm. This reactor is placed in an electric furnace with heating ramp and controlling the temperature by means of a controller.

At the top is inserted the gas inlet duct and a K-type thermocouple to measure the temperature of the catalytic bed (0.25 g of fresh catalyst on which 1.44 g of SiC was added to avoid the formation of hot spots). Gases leaving the reactor were analysed using a gas chromatograph, Varian 450, equipped with a thermal conductivity detector and two capillary columns in series: a Msieve-5A molecular sieve for the analysis of permanent gases (H_2, O_2, N_2 CO and CH_4) and a PoraBOND Q packed column allowing the separation of polar compounds (methanol, dimethyl ether, water and CO_2).

The measurement procedure consists of two steps, an activation step and a successive reaction step. In the first one, the formation of the PdZn alloy, the active phase of the catalysts, was carried out by in situ reduction with a current of 50 mL(N)/min of Ar and 5.56 mL(N) min^{-1} of H_2 under the selected conditions (450 °C, 5 °C·min^{-1}, 1 h). Subsequently, activity measurements were performed in the reaction step. Once the reaction temperature was reached (250 ºC) and after feeding the system with a flow of 50 mL(N) min^{-1} of the feed stream (21.3% CO_2, 64% H_2 and 14.7% N_2), it was pressurized until reaching 30 bar. Measurements were performed over a period of 8 h. The catalytic tests were conducted under high space-velocity (GHSV=12000 $mL_{CO2/H2}$ $g_{cat}^{-1}h^{-1}$) to achieve low conversions (< 3%) to exclude the effect of equilibrium and to better visualize the differences in activity and deactivation.

The behaviour of the catalysts was measured in terms of CO_2 conversion, methanol and CO yield (mmol CH_3OH/min mole of Pd) and selectivity to CO and methanol, taking into account the reactions that can occur during the hydrogenation of the CO_2 (Eqs. 1–4) and applying the corresponding mass balances.

$$CO_2 + 3H_2 \rightarrow CH_3OH + H_2O \quad (1)$$

$$CO_2 + H_2 \leftrightarrow CO + H_20 \quad (2)$$

$$CO_2 + 4H_2 \rightarrow CH_4 + 2H_2O \quad (3)$$

$$2CH_3OH \rightarrow CH_3OCH_3 + H_2O \quad (4)$$

To calculate these parameters (Eqs. 5–7), the proportions of the outlet gases were determined from the analysis of the relative areas obtained by integration of the chromatograms, taking N_2 as the internal standard.

$$CO_2 \quad conversion \quad = \frac{CO_2 \quad out - CO_2 \quad in \quad (mol/min)}{CO_2 \quad in \quad (mol/min)} \times 100 \quad (5)$$

$$CH_3OH \quad (CO) \quad production = \frac{CH_3OH \quad (CO) \quad out \quad (mol/min)}{Pd \quad in \quad catalyst \quad (mol)} \times 100 \quad (6)$$

$$CH_3OH \quad (CO)(\%) \quad selectivity = \frac{CH_3OH \quad (CO) \quad out \quad (mol)}{total \quad products \quad (mol)} \times 100 \quad (7)$$

3. Results and discussion

3.1. Physicochemical characterization of calcined PdZn/Ti catalysts

3.1.1. Chemical analysis and structural properties

The elemental composition of the TiO_2 support and PdZn/Ti calcined catalysts was determined by ICP-OES (Table 1). As can be seen in Table 1, the experimental values of Pd and Zn concentrations are very close to nominal ones, indicating the efficiency of the impregnation method.

The structure of the crystalline phases present in the calcined catalysts was investigated by X-ray diffraction. XRD profiles of the TiO_2 support and calcined PdZn/Ti catalysts are collected in Fig. 1A. As expected, the TiO_2 support and the calcined catalysts show intense diffraction peaks at 2θ 25.3º (101), 36.9º (103), 37.8º (004), 38.6º (112), 48.1º (200), 53.9º (105) and 55.1º (211) corresponding to the tetragonal crystal system of the anatase phase of TiO_2 (space group *I*41/amd, JCPDS 01–021–1272). It is observed that the incorporation of PdO and ZnO does not alter the diffraction profiles of the anatase phase of the TiO_2 support. Diffraction lines at 2θ 31.7º, 34.4º, 36.3º and 56.6º, also appear in the profiles of the calcined catalysts corresponding to (100), (002), (101) and (110) planes of the hexagonal würtzite-type crystal structure of ZnO (space group *P*63mc, JCPDS 01–071–1169. An increase in the intensity of the diffraction peaks associated with the ZnO crystalline phase is observed as the Zn loading increases in PdZn/Ti catalysts. However, the intensity of the diffraction peaks of the ZnO phases is not very high in any of the PdZn/Ti catalysts, indicating small particle size and/or low crystallinity of the ZnO particles in all samples. Finally, all the calcined catalysts also show two broad and poorly defined diffraction peaks at 33.8º and 41.9º corresponding to (101) and (110) planes of the tetragonal crystal structure of poorly crystallized palladium oxide (space group *P*42/mmc, JCPDS 00–041–1107). The intensity of the diffraction peaks associated with PdO decreases as the Zn loading on the catalysts increases, reflecting a loss of crystallinity or increased

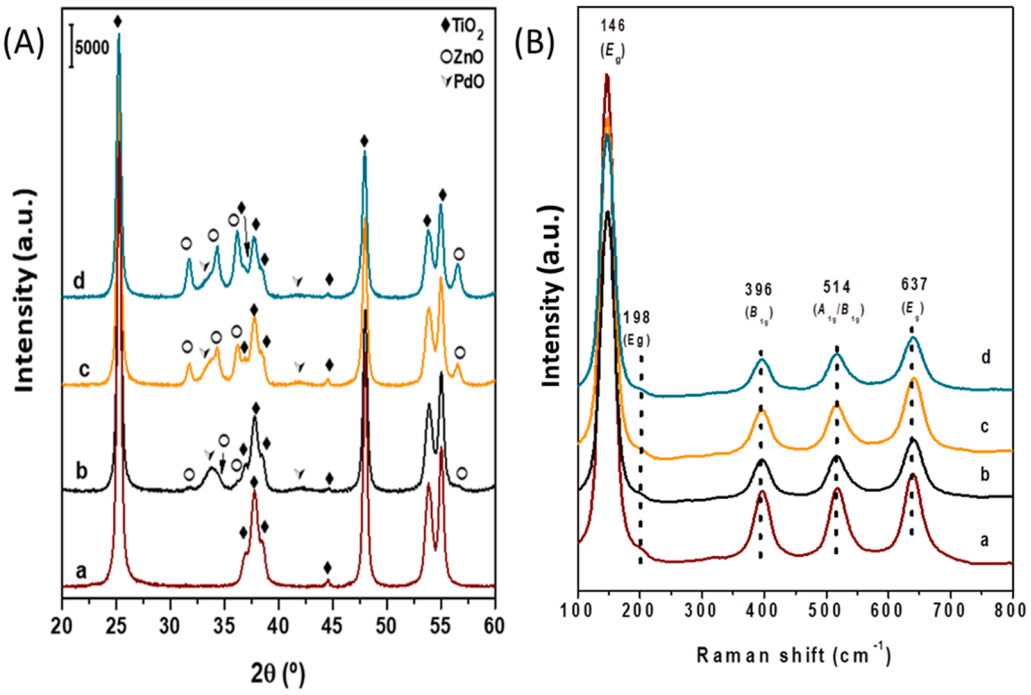

Fig. 1. X-ray diffraction profiles (A) and Raman spectra (B) of the TiO_2 support (a) and calcined PdZn/Ti catalysts with a Zn/Pd molar ratio of 2.5 (b), 5 (c) and 7.5 (d).

dispersion of the PdO particles (size < 4 nm) associated with the increase of Zn in the samples.

The crystalline domain sizes of TiO_2 and ZnO phases in PdZn/Ti catalysts, determined from the Scherrer equation applied to the diffraction peaks at 25.3° ((101), anatase) and 31.8° ((100), ZnO) are given in Table 2. The crystallite size of the PdO phase could not be calculated for any of the calcined catalysts because of the overlap of the diffraction peak of poorly crystaline PdO at 41.9° with the diffraction peak of ZnO (34.4°). The data in Table 2 show that the crystallite size of the anatase phase of the TiO_2 support is not changed after the incorporation of PdO and ZnO in the calcined catalysts. It is also observed that all the calcined catalysts exhibit ZnO particles with low crystallite size that slightly increases (from 11.9 to 14.6 nm) when the Zn loading in the catalysts increases.

The vibrational modes of the anatase and ZnO phases in the support and calcined PdZn/Ti catalysts were investigated by Raman spectroscopy (Fig. 1B). Titania support shows bands at 146 cm^{-1} (symmetric stretching of Ti-O-Ti bonds), 198 cm^{-1}, 396 cm^{-1} (symmetric bending vibrations), 514 cm^{-1} and 637 cm^{-1} that are associated with E_g, $B_{1\,g}$, $A_{1\,g}/B_{1\,g}$ and E_g Raman modes of anatase TiO_2 crystals, respectively, [51]. As can be seen in Fig. 1B, all calcined catalysts exhibit the same bands as those observed on the TiO_2 support. The absence of changes in the intensity or vibrational mode shifts in the Raman bands of anatase in the calcined PdZn/Ti catalysts excluded surface disorder due to the formation of oxygen vacancies or non-stoichiometric defects after incorporation of the PdO and ZnO species on the TiO_2 support [52]. ZnO wurtzite with P63mc symmetry should show small Raman peaks located at 332, 379 and 437 cm^{-1} assigned to its $2E_2$, $A_1(T_o)$ and E_2 (high) vibrational modes [53]. However, no bands corresponding to crystalline ZnO species are observed in any of the calcined catalysts. Raman signals are usually very sensitive to structure as well as crystal defects and therefore the absence of Raman peaks associated with hexagonal ZnO particles corroborated the low crystallinity of ZnO particles already detected by XRD on all calcined PdZn/Ti catalysts. However, in contrast to visible Raman spectra, the presence of ZnO particles decorating the surface of the PdZn/Ti-7.5 catalyst have been observed by UV Raman spectroscopy. This is because fluorescence interference does not normally occur in the UV region. After pretreatment of the PdZn/Ti-7.5 catalyst with air at 350 °C for 1 h, bands at 575 and 1160 cm^{-1} characteristic of ZnO particles [54] were observed (spectra not shown here).

Table 2
Textural parameters (BET area, volume and main pore size) of TiO_2 support and calcined PdZn/Ti catalysts.

	S_{BET} (m^2/g)	S_{BET} (m^2/g TiO_2)	V_{total} (cm^3/g)	V_{total} (cm^3/g TiO_2)	d_{pore} (nm)
TiO_2	74	74	0.29	0.29	14.0
PdZn/Ti-2.5	64	72	0.26	0.29	14.0
PdZn/Ti-5	64	79	0.24	0.30	13.0
PdZn/Ti-7.5	63	87	0.21	0.29	10.9

3.1.2. *Textural properties*

The textural characteristics of the TiO_2 support and calcined PdZn/Ticatalysts were determined from their N_2 adsorption-desorption isotherms (Fig. 2). According to the IUPAC classification [55], the TiO_2 support and calcined catalysts show type IV isotherms, characteristic of mesoporous solids. All isotherms show H1-type hysteresis loop characteristic of porous systems with uniform particle size and distribution. It is noteworthy that there is no significant difference in the shape of the N_2 adsorption-desorption isotherms of the calcined PdZn/Ti catalysts in spite of Zn loading variation. A decrease in the maximum volume of N_2 adsorbed at a relative pressure of 0.99 is observed for all calcined PdZn/Ti catalysts, as corresponds to the dilution effect due to the Zn loading. The textural parameters of the calcined catalysts were calculated from its isotherms and compared with the TiO_2 support. Taking into account the dilution effect of the TiO_2 support caused by the variation of Pd and Zn loadings, the textural parameters listed in Table 2 were normalized per gram of TiO_2 in each sample. The normalized specific surface areas of calcined PdZn/Ti catalysts are similar (PdZn/Ti-2.5) to or higher (PdZn/Ti-5 and PdZn/Ti-7.5) than that of the bare TiO_2 support. It is observed a linear correlation between the BET

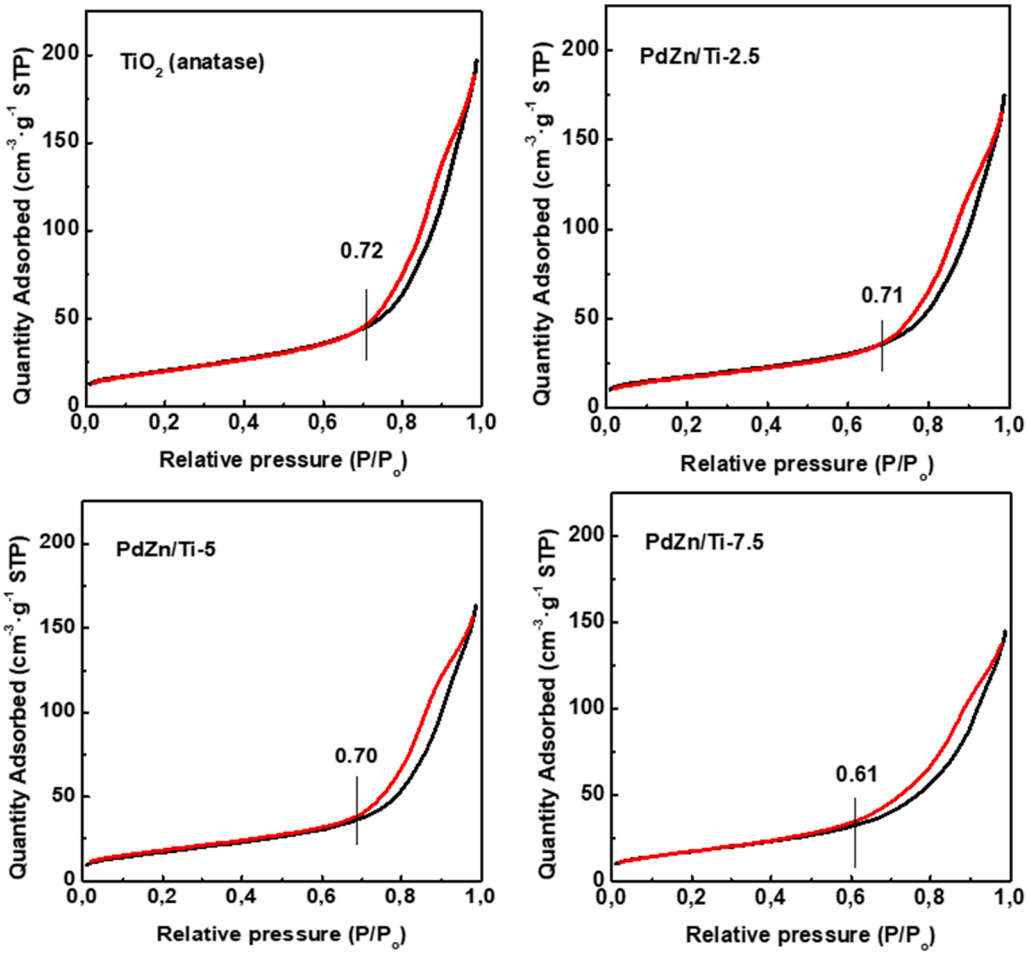

Fig. 2. N_2 adsorption-desorption isotherms (marked in black and red, respectively) for TiO_2 support and calcined PdZn/Ti catalysts.

specific surface area normalized per g of TiO_2 and the Zn loading (Fig. 3A) which indicates that most of the ZnO particles segregate from support developing surface area. Consistent with this fact, the small change in normalized pore volume (Table 2) or pore size distribution (Fig. 3B) with variation of Zn loading in the calcined catalysts indicates no blockage of the pore openings of the TiO_2 support and corroborates that most of the ZnO was not inside the porous structure of the support. Therefore, the increase in the normalized surface area observed in catalysts with higher Zn loading (PdZn/Ti-5 and PdZn/Ti-7.5) is associated with the larger contribution of the specific surface area of the ZnO

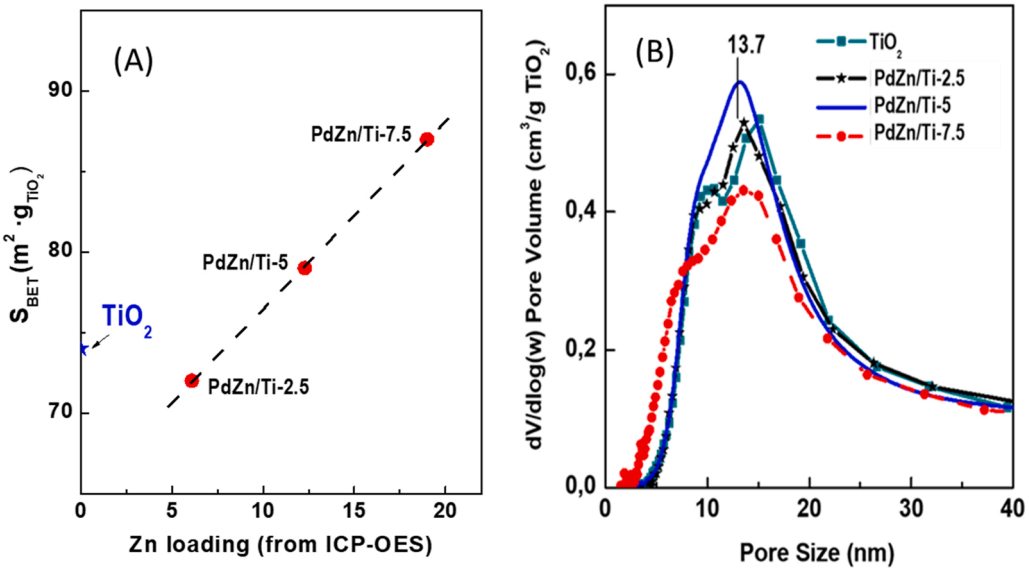

Fig. 3. Specific catalyst surface area versus Zn loading (A) and pore size distribution of calcined PdZn/Ti catalysts (B).

nanoparticles segregated outside of the porous structure of the TiO_2 support.

3.1.3. H_2-Temperature programmed reduction

Reducibility of PdO and ZnO species in calcined PdZn/Ti catalysts were studied by temperature programmed reduction and the hydrogen consumption profiles are shown in Fig. 4. All calcined catalysts show a main reduction peak between 25 and 50 °C corresponding to the reduction of small particles of PdO which is consistent with the results published in the literature that show the easier reduction of smaller PdO particles by hydrogen due to its higher relative surface to reduce [56]. In none of the reduction profiles of calcined PdZn/Ti catalysts appears the negative peak associated to H_2 desorption by decomposition of the palladium hydride (PdH_x) formed through hydrogen diffusion into metallic Pd particles [46,57]. The absence of this negative peak is due to the fact that the formation temperature of the palladium hydride (room temperature) is lower than that corresponding to the reduction of the small PdO particles observed in calcined PdZn/Ti catalysts [58]. The reduction temperature of PdO particles in calcined PdZn/Ti catalysts changes slightly with Zn content. The PdZn/Ti-7.5 catalyst shows a shift in the reduction peak maxima from 38° to 27°C, indicating an easier reduction of PdO particles compared to PdZn/Ti-2.5 and PdZn/Ti-5 catalysts, which is probably associated with the differences in PdO particle size already observed by XRD. In addition to the reduction peak of PdO, calcined PdZn/Ti catalysts show additional hydrogen consumption peaks in the temperature range between 300 and 425 °C (inset of Fig. 4). The consumption peak in this temperature range is associated with the partial reduction of ZnO, assisted by the mechanism of hydrogen spillover on metallic Pd particles, to form the intermetallic PdZn compound [36,59]. This mechanism occurs when molecular hydrogen dissociates on the surface of palladium metal and atomic hydrogen spilled from Pd^0 to the Pd-ZnO interface, leading to the partial reduction of ZnO. Then, the low-valence species $Zn^{(2-\delta)+}$ ($0 < \delta < 2$) together with the electron-poor active sites ($Pd^{\delta+}$) form the intermetallic PdZn compound [60]. The intensity of hydrogen consumption peaks associated with the reduction of Zn species was similar for all calcined PdZn/Ti catalysts (Fig. 4), which seems to indicate similar ZnO reduction and intermetallic PdZn formation in the PdZn/Ti samples. Slight differences are observed, however, in the temperature at which the maximum reduction of Zn species appears in the calcined catalysts. With

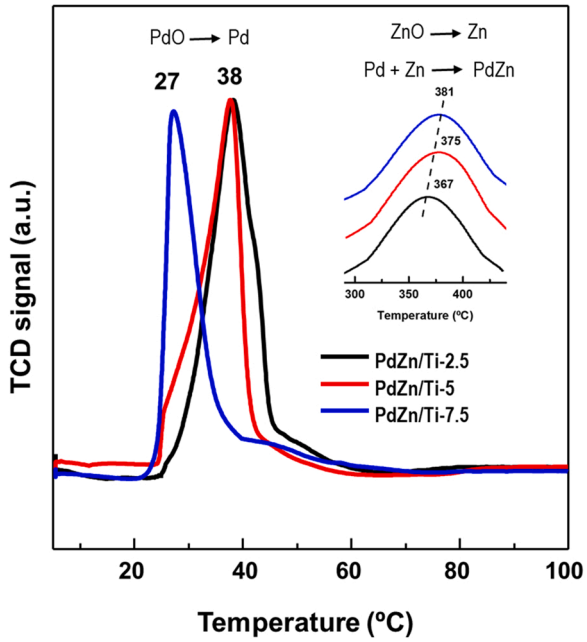

Fig. 4. H_2-TPR profiles of calcined PdZn/Ti catalysts.

increasing the Zn loading in calcined catalysts, the maximum of the reduction peak of ZnO species shifts from 367 (PdZn/Ti-2.5) to 387 °C (PdZn/Ti-7.5) and this shift can be considered as a consequence of the increase in the number and crystallinity of ZnO particles, in agreement with the above XRD data.

3.2. Characterization of reduced PdZn/Ti catalysts

3.2.1. Structural (XRD) characterization

The formation and evolution of the PdZn intermetallic phase during the hydrogen reduction of PdZn/Ti catalysts at different temperature were studied by in situ XRD. Fig. 5 shows the evolution of the X-ray diffraction profiles of the PdZn/Ti catalysts with increasing the reduction temperature. The reduction of PdZn/Ti catalysts at 50 °C leads to the disappearance of the diffraction peak attributed to the PdO phase and to the simultaneous growth of a diffraction peak at 40.1° corresponding to (111) plane of Pd metal phase with cubic structure (space group *F*m3 m, JCPDS-046–1043). This is in agreement with previous H_2-TPR results showing that PdO reduction occurs between 25 and 50 °C (Fig. 4). The crystalline domain sizes of Pd in PdZn/Ti catalysts reduced at 150 °C, determined from the Scherrer equation, show the formation of small crystalline domains of Pd whose size slightly decreases with increasing Zn loading on the catalyst (PdZn/Ti-2.5 =5.5 nm, PdZn/Ti-5 =5.9 nm, PdZn/Ti-7.5 =4.8 nm). The diffraction peak assigned to metallic palladium remains stable up to 250 °C and, from that temperature a shoulder appears at 41.2° attributed to (111) plane of the intermetallic β-PdZn phase with the tetragonal crystal structure (space group *P*4/mmm, JCPDS 00–006–0620), indicating the beginning of the formation of PdZn by the incorporation of reduced zinc atoms into the metallic palladium lattice [61]. In the case of the PdZn-5 catalyst, the peaks at 2Θ of about 41.2° and 44.1° are identical to the planes of (111) and (200), respectively, of the β-PdZn crystal. In addition to this PdZn intermetallic phase, the PdZn/Ti-2.5 and PdZn/Ti-5 catalysts reduced at temperatures above 100 °C exhibit a peak at 2Θ 44.6° (Fig. 5). This peak is characteristic of the (004) plane of the cubic zinc blende crystalline phase (space group *F*m3m, JCPDS. 77–0191) [62–64]. The intensity of this peak increases with increasing the reduction temperature indicating the growth of the cubic ZnO blende phase. It is known that the zinc blende ZnO structure is metastable and can be only stabilized by heteroepitaxial growth on cubic substrates [65]. Therefore, the presence of this ZnO blende crystalline phase in the PdZn/Ti-2.5 and PdZn/Ti-5 catalysts reflect the thermal growth of well-dispersed ZnO nanoparticles in close contact with cubic Pd particles. Unlike PdZn/Ti2.5 and PdZn/Ti-5, the PdZn/Ti-7.5 sample did not show the formation of the ZnO blende phase because the bigger ZnO particles in this case led to the sintering of the ZnO hexagonal wurtzite phase, as deduced from the increase in the intensity of the diffraction peak at 36.3° as the reduction temperature increases.

The increase of the reduction temperature from 250° to 450°C leads to an increased formation of β-PdZn intermetallic species, as can be seen from the increase of the reflection intensity at 41.2°, and the appearance of the second main diffraction peak near 44.1°. All PdZn/Ti catalysts show similar evolution of their XRD diffraction profiles during reduction, with no significant differences in the initial temperature for the formation of the β-PdZn phase. However, diffraction peaks intensities of the intermetallic β-PdZn species are different as a function of the Zn loading in the catalysts. PdZn/Ti-5 presents peaks of higher intensity indicating better developed crystallinity.

The crystalline domain sizes of TiO_2, ZnO and β-PdZn phases in PdZn/Ti catalysts reduced at 450 °C, determined from the Scherrer equation, are given in Table 5. Compared to calcined PdZn/Ticatalysts, TiO_2 support particles do not undergo significant alterations in crystallinity or size after reduction at 450 °C. The data summarized in Table 5 indicate that all reduced PdZn/Ti catalysts show β-PdZn particles with low crystallite size (around 5–6 nm) and that this crystallite size slightly decreases with increasing Zn loading following the same trend observed

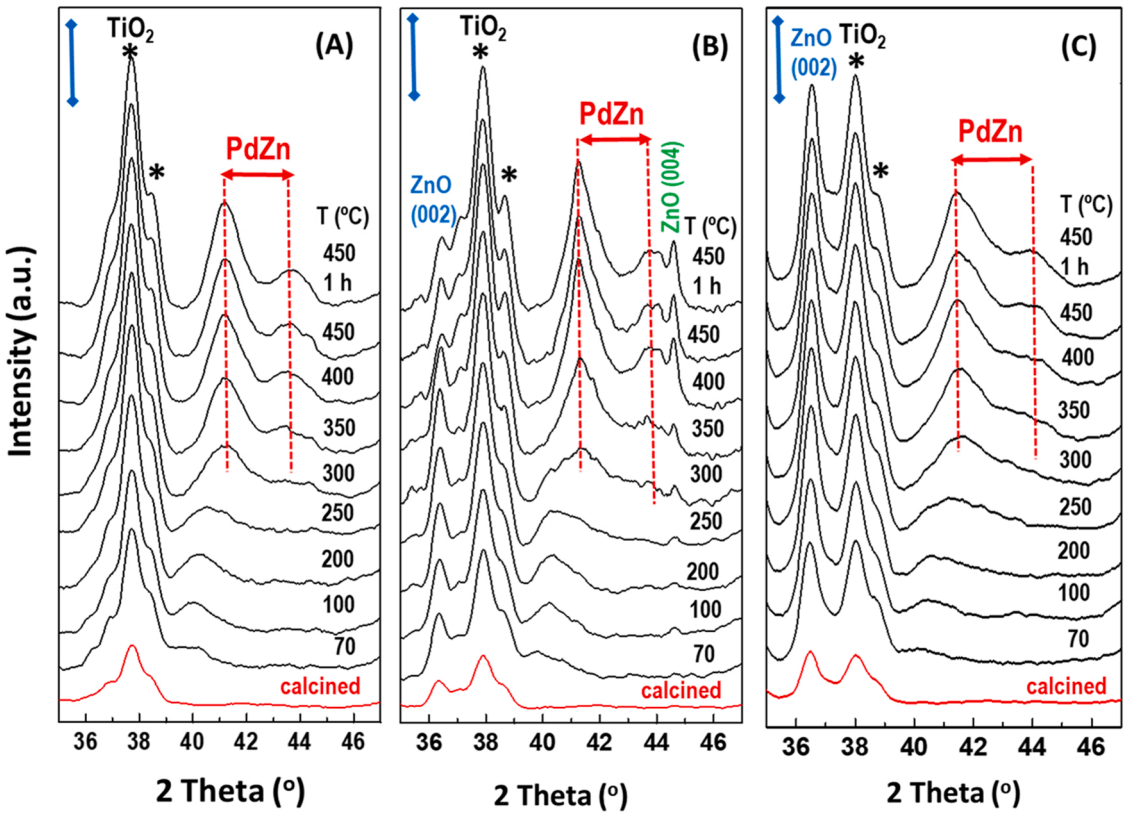

Fig. 5. X-ray diffraction profiles of the PdZn/Ti catalysts in situ reduced at different temperatures under H_2/Ar (10% vol. H_2): (A), PdZn/Ti-2.5. (B), PdZn/Ti-5, and (C), PdZn/Ti-7.5.

for Pd particles after low-temperature reduction. To evaluate the growth direction of ZnO crystallites, their crystallite size was calculated considering the (100), (002) and (101) crystal planes of this phase. For reduced catalysts, the ZnO crystallite size shows a reduction in the PdZn/Ti-5 and PdZn/Ti-7.5 samples, although it is more pronounced in the former. The size along the polar facet (002) of ZnO also changes after reduction showing an increase in this direction when the Zn loading on the PdZn/Ti catalysts increases.

3.2.2. CO-DRIFTS

For the Pd/TiO_2 and PdZn/Ti catalysts, the evolution of chemical state of Pd sites during hydrogen reduction at different temperatures was investigated by DRIFT spectroscopy of adsorbed CO, since this probe molecule interacts differently with metallic Pd^0 and intermetallic PdZn sites (π-donation at Pd sites and σ-donation at PdZn sites) [66,67]. The PdZn/Ti catalysts reduced at 70 °C (Fig. 6A) show absorption bands at 2059–2072 cm^{-1}, 1965 cm^{-1} and 1870–1877 cm^{-1}. They can be assigned to linear CO-Pd^0 and bridged CO at Pd edges/corners and Pd (111) facets, respectively [68,69]. The presence of two bridge-bound CO peaks is typical of pure Pd catalysts. All PdZn/Ti catalysts reduced at 70 °C show a higher amount of CO bridged-bound species than linearly adsorbed species, consistent with the crystallite size of Pd nanoparticles in the reduced catalysts determined by XRD (4–6 nm). The ratio of bridged/linear species in the reduced PdZn/Ti samples (Fig. 5A) decreases as the Zn loading on the catalysts increases, suggesting a smaller size of Pd, which is in agreement with previous XRD data (Fig. 5). In addition, the linearly adsorbed CO band shifts to a lower wavenumber (2056 cm^{-1}), indicating higher CO adsorption at edge sites. As expected, CO adsorption on Pd/TiO_2 occurs differently from that on PdZn/Ti catalysts reduced at 70 °C (Fig. 6A). When CO is adsorbed on the monometallic Pd/TiO_2 catalyst, two bands at 1836 and 1964 cm^{-1} associated with bridged CO are observed [70]. It is noteworthy that, unlike the PdZn/Ti catalysts, the Pd/TiO_2 catalyst shows a very low

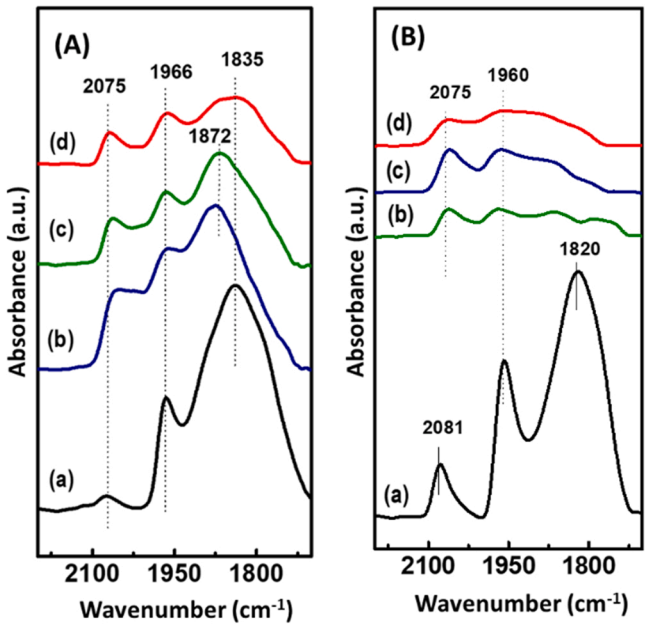

Fig. 6. DRIFT spectra of adsorbed CO over Pd/TiO_2 and PdZn/Ti catalysts reduced at 70 °C (A) and 250 °C (B): (a), Pd/Ti; (b), PdZn/Ti-2.5; (c), PdZn/Ti-5 and (d), PdZn/Ti-7.5.

amount of CO terminally bound to the Pd sites (linear adsorption of CO), as deduced from the very small intensity of the band centred at 2075 cm^{-1}. Compared to Pd/TiO_2, PdZn/Ti catalysts show much lower intensity of CO bands at wavenumbers below 2000 cm^{-1}. This can be explained by considering a dilution effect of Zn and/or better dispersion

of Pd on ZnO in PdZn/Ti catalysts, since the CO adsorption intensity below 2000 cm^{-1} decreases with increasing Zn/Pd ratio. This inhibition in the adsorption of CO bridging over the Pd sites associated with the presence of Zn on the PdZn/Ti catalysts, is in agreement with the observations of Araña et al. [70]. As compared to the catalysts reduced at 70 ºC, DRIFT-CO spectra of all catalysts reduced at 250 ºC are different (Fig. 6B). The monometallic Pd/TiO_2 catalyst shows very low linear adsorption of CO, as deduced from the very small intensity of the band at 2075 cm^{-1}, suggesting the presence of large Pd particles on the surface of this catalyst. In contrast to Pd/TiO_2, for PdZn/Ti catalysts the CO absorption in the region of CO bridging strongly decreased. For PdZn/Ti catalysts, the formation of the PdZn alloy can be deduced from a decrease in band wavenumber from 2081 cm^{-1} to 2075 cm^{-1} due to terminal CO when comparing the Pd/TiO_2 with the PdZn/Ti catalysts (Fig. 6B).

The formation of the intermetallic PdZn phase during the reduction of PdZn/Ti catalysts was evaluated from the evolution of CO-DRIFTS spectra of the catalysts reduced at 70, 250, 350, 400 and 450 °C (Fig. 7B-7D). The increase in the reduction temperature from 70° to 250°C leads to a decrease in the intensity of the CO adsorption bands in all PdZn/Ti catalysts and this decrease in intensity is particularly important for the bridged CO species. The literature reports the reduction of bridged CO species with the formation of intermetallic PdZn due to the ensemble effect, as the enlargement of the distance between two palladium atoms occurs when Zn is incorporated [71,72]. Furthermore, the bands corresponding to linear CO in all PdZn/Ti catalysts after reduction at 250 °C are red-shifted compared to the catalysts reduced at 70 °C, indicating a modification of the electronic properties of palladium in accordance with the formation of intermetallic PdZn (electron transfer from Zn to Pd leads to increased back-donation from Pd to CO). Comparison of band intensities in the CO-DRIFT spectra of the PdZn/Ti catalysts after reduction at 250 °C suggests an increased intermetallic PdZn formation with increasing Zn loading on the catalysts. The intensity of adsorbed CO after the formation of intermetallic PdZn decreases with reduction temperature and this decrease is more pronounced as the Zn loading in PdZn/Ti catalysts increases. The CO adsorption on PdZn/Ti-5 and PdZn/Ti-7.2 after reduction at 450 ºC drop to near zero due to a massive decrease by alloying [73].

3.2.3. HRTEM microscopy

The nanomorphology and chemical state of PdZn/Ti catalysts after reduction at 450 °C were analyzed by HRTEM microscopy. Representative TEM images of reduced PdZn/Ti catalysts (at 450 ºC) and the corresponding histograms of particle size distribution are shown in Fig. 8. All TEM images of the reduced catalysts show PdZn, ZnO and TiO_2 nanoparticles. TEM images of PdZn/Ti catalysts show intermetallic PdZn nanoparticles with pseudo-spherical morphology with better dispersion and contact with ZnO particles as the Zn concentration in the catalysts increases. Statistical analysis of the size of the PdZn nanoparticles suggests that the catalyst with the highest Zn content (PdZn/Ti-7.5) exhibits a narrower particle size distribution than the PdZn/Ti-2.5 and PdZn/Ti-5 counterparts. The mean crystallite size of intermetallic PdZn follows the trend: PdZn/Ti-5 (6.7 nm) > PdZn/Ti-2.5 (5.5 nm) > PdZn/Ti-7.5 (4.7 nm). In the case of PdZn/Ti-7.5, about 75% of the particles are between 3 and 5 nm in size. The size of the PdZn crystallites determined by TEM agrees relatively well with the XRD results (Table 5), which excludes the formation of large crystalline aggregates of PdZn.

Figs. 9–11 shows selected HRTEM images of reduced PdZn/Ti catalysts and their corresponding fast Fourier transform (FFT) analysis zones. The TiO_2 phase of all PdZn/Ti catalysts was well crystallized and FFT images indicated crystalline d-spacing of 0.35 nm corresponding to (101) crystal planes for TiO_2 anatase phase, in good agreement with XRD results (Fig. 1A). The formation of crystalline intermetallic PdZn on reduced PdZn/Ti catalysts was proved by inverse FFT analysis showing all reduced PdZn/Ti catalysts the lattice fringes of 0.219 and 0.205 nm, which are characteristic of the (111) and (200) faces of the intermetallic β-PdZn (JCPDS 00–006–0620), respectively. In contrast to the crystalline well defined intermetallic β-PdZn particles, the ZnO particles in reduced PdZn/Ti catalysts exhibit poor crystallinity, in good agreement with XRD (Fig. 5) and Raman spectroscopy characterization (Fig. 1B). The lattice of ZnO is hardly visible in HTEM images and is only observed on the catalysts with higher ZnO loading, PdZn/Ti-5 and PdZn/Ti-7.5 (Figs. 10 and 11). In these samples, FFT images of ZnO particles indicate a dd-spacing-spacing of 0.26 nm associated to the (002) plane of the ZnO phase. HRTEM images of PdZn/Ti-5 and PdZn/Ti-7.5 samples also show intimate contact between the β-PdZn and ZnO particles as the Zn loading on the catalysts increases (Figs. 10 and 11). HRTEM images of

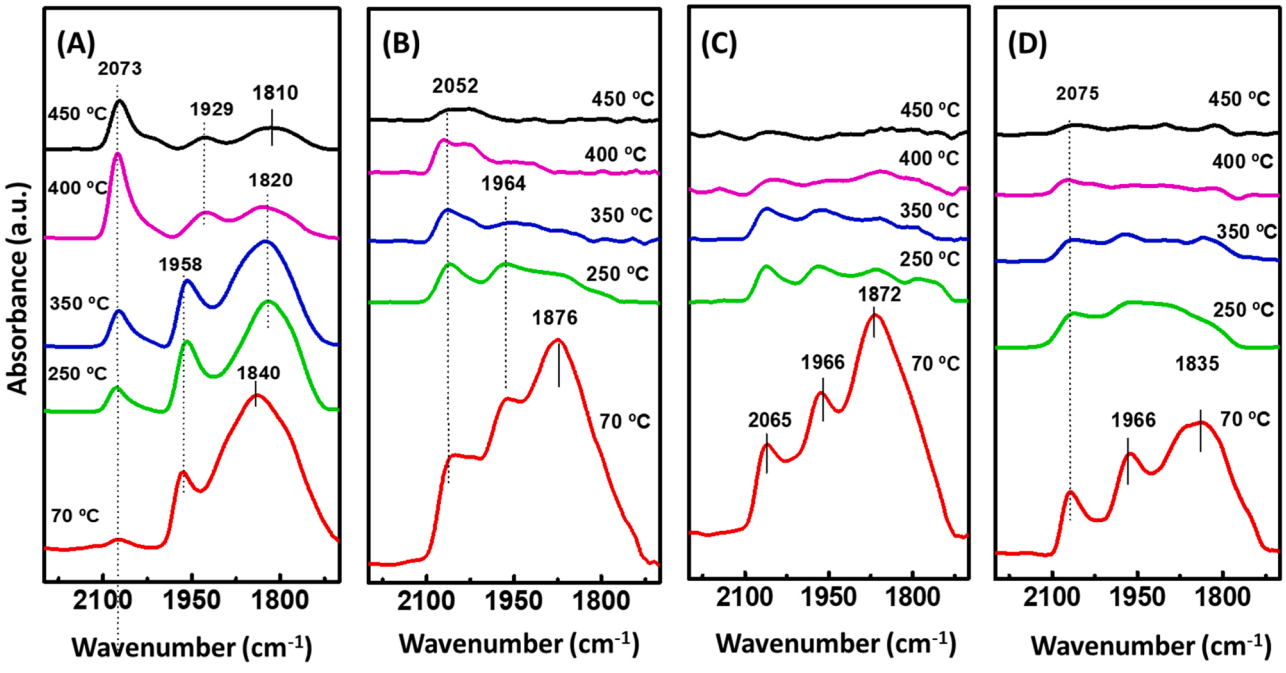

Fig. 7. DRIFT spectra of adsorbed CO over catalysts reduced at different temperatures: (A), Pd/TiO_2; (B), PdZn/Ti-2.5; (C), PdZn/Ti-5 and (D), PdZn/Ti-7.5.

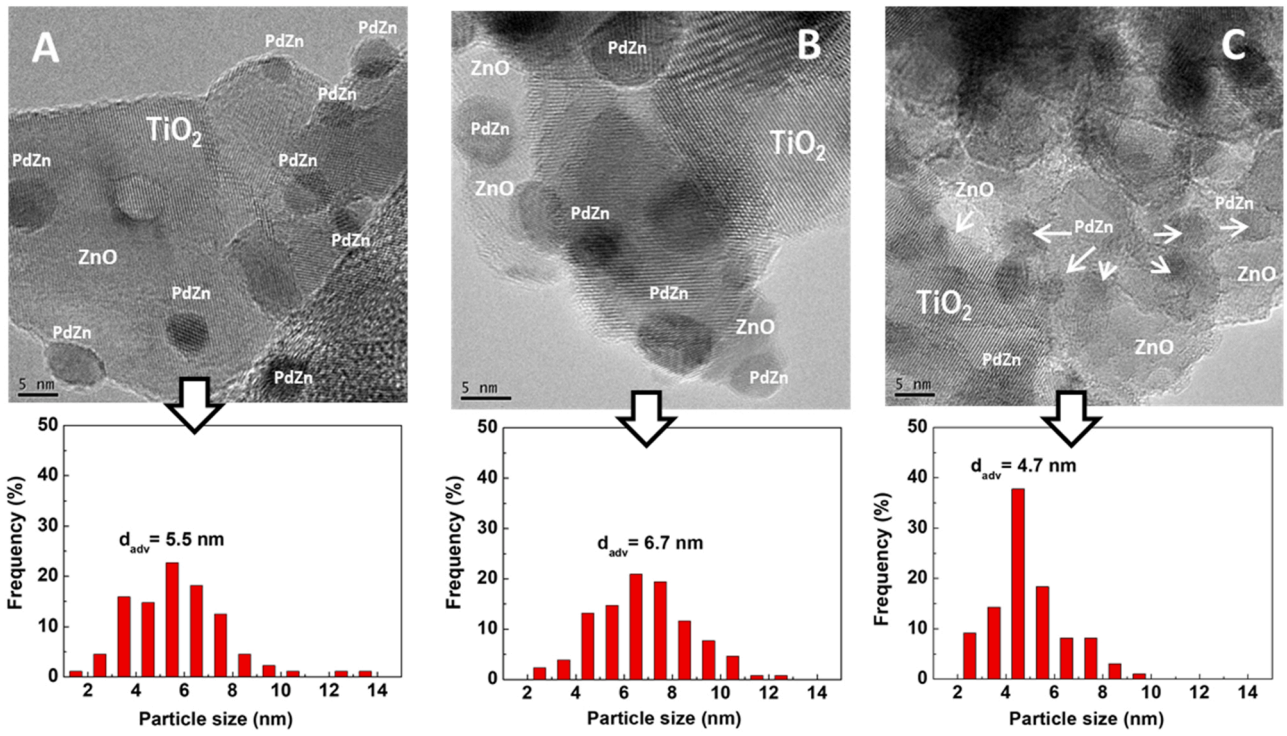

Fig. 8. TEM images and particle size distribution of intermetallic β-PdZn of reduced PdZn/Ti catalysts: (a), PdZn/Ti-2.5; (b), PdZn/Ti-5, and (c), PdZn/Ti-7.5.

PdZn/Ti-5 and PdZn/Ti-7 samples show intimate contact between PdZn and ZnO, PdZn on top and right next of the ZnO nanoparticles. The formation of the intermetallic phase is only possible in cases where the metallic Pd is on top and/or right next of the ZnO nanoparticle to it, as confirmed by HRTEM images (Figs. 9 and 10).

3.2.4. H_2-Temperature programmed desorption

Fig. 12 shows the temperature-programmed desorption profiles of hydrogen adsorbed on the reduced PdZn/Ti catalysts. As can be seen, all the reduced PdZn/Ti catalysts show very large hydrogen desorption in the temperature range from 30 °C to 374 °C. Literature studies on H_2 adsorption on intermetallic PdZn are scarce and suggest that the higher the degree of formation and the size and crystallinity of intermetallic PdZn, the higher the amount and temperature of hydrogen desorption [17,74]. All reduced PdZn/Ti catalysts showed a very similar amount of desorbed hydrogen, indicating, in agreement with previous characterization results, a similar formation of intermetallic PdZn in all samples. However, differences are observed in the temperature at which hydrogen desorbs in reduced PdZn/Ti samples. The PdZn/Ti-7.5 catalyst with the highest Zn loading desorbs hydrogen at lower temperature (87 °C) than the PdZn/Ti-5 and PdZn/Ti-2.5 catalysts with lower ZnO content (157 and 164 °C, respectively), indicating lower adsorption of hydrogen species on the intermetallic PdZn as the Zn loading on the catalyst increases. This fact is also consistent with the studies discussed above, as the desorption temperature sequence observed for PdZn/Ti catalysts coincides with the particle size variation of the intermetallic PdZn on the catalysts determined by XRD and HRTEM (Table 5 and Fig. 8, respectively).

3.3. Catalytic Activity

Fig. 13 A shows the activity data (methanol yield per mol of Pd) corresponding to the direct synthesis of methanol from CO_2/H_2 on PdZn/Ti catalysts reduced at 450 ºC. Under the mild reaction conditions employed (250 °C, 30 bar, GHSV=12,000 $mL_{CO2/H2}$ $g_{cat}^{-1}h^{-1}$) the only products detected in all tests were CH_3OH, CO and H_2O, with no hydrocarbon production. It is observed that all the PdZn/Ti catalysts maintain the methanol yield during the reaction period and even a slight increase in yield is observed with reaction time for the samples PdZn/Ti-5 and PdZn/Ti-7.5. Table 3 shows the CO_2 conversion, methanol selectivity and methanol yield data of Pd/Ti and PdZn/Ti catalysts after 8 h of time-on-stream (TOS). It is observed that the CO_2 conversion and selectivity toward methanol depend on the Zn loading on the PdZn/Ti catalysts. The CO_2 conversion increases as the Zn loading on the catalysts increases, while the selectivity towards methanol reaches the maximum for the sample with the intermediate Zn content (PdZn/Ti-5) and decreases for the sample with the highest Zn content (PdZn/Ti-7.5). As can be seen, the methanol yield on the PdZn/Ti catalysts increases when the Zn content in the catalysts increases: PdZn/Ti-7.5 (78.9 $mmol_{CH3OH}·min^{-1}·mol_{Pd}^{-1}$) > PdZn/Ti-5 (30.3 $mmol_{CH3OH}·min^{-1}·mol_{Pd}^{-1}$) > PdZn/Ti-2.5 (13.1 $mmol_{CH3OH}·min^{-1}·mol_{Pd}^{-1}$). From this result it is clear that Zn loading plays an important role in the catalytic activity, presumably by promoting the interaction of intermetallic PdZn particles with ZnO to induce methanol formation. As compared to the PdZn/TiO_2 catalysts, the monometallic Pd/TiO_2 reference catalyst showed much higher CO_2 conversion, but no methanol formation (Table 3). Instead of methanol, CO was formed with a selectivity of 96%. This is due to the well-known ability of Pd to catalyze the RWGS reaction [32].

There are not many previously published works on the synthesis of methanol from CO_2 over PdZn catalysts. Moreover, the published activity measurements have been carried out over a wide range of pressures and temperatures, which makes comparisons between catalysts difficult. Therefore, Table 4 compares the efficiency of the most active catalyst tested in this work, PdZn/Ti-7.5, with published PdZn catalysts measured under the same temperature and pressure as those used in our tests (T = 250 °C and P = 30 bar) [21,30,75]. It is observed that the methanol yield value per gram of Pd, a way to normalize the activity per active Pd metal in the comparison of catalysts tested with different space velocity and Pd loading, over the PdZn/Ti-7.5 was similar to the most active PdZn catalysts reported in the literature under similar reaction conditions. The catalyst reported by Song et al. [30] shows one of the

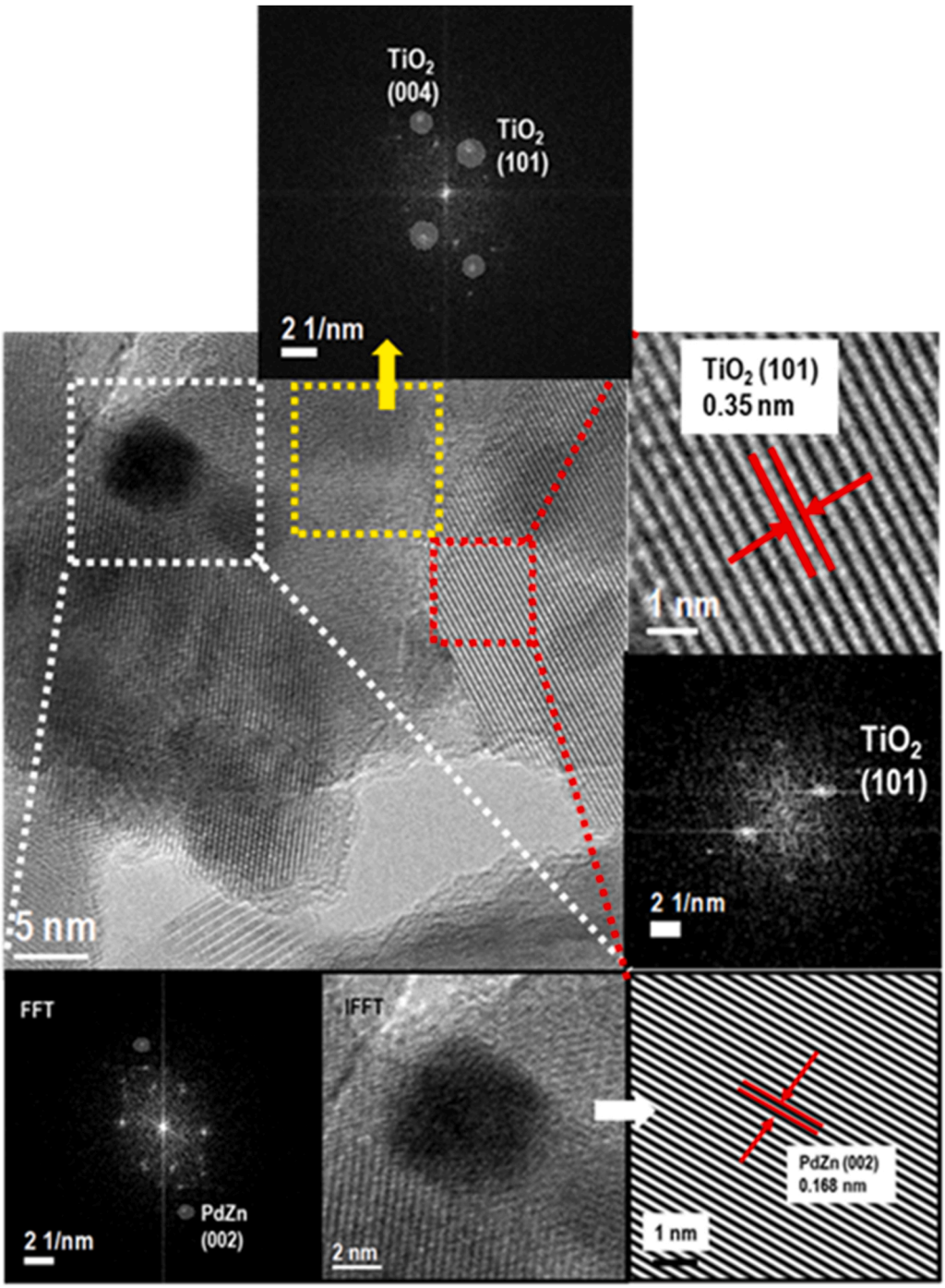

Fig. 9. HRTEM images of reduced PdZn/Ti-2.5 catalyst and corresponding FFT and IFFT images of individual PdZn and TiO_2 particles.

highest methanol yield for methanol synthesis from CO_2 in the literature. This catalyst shows a higher methanol yield per gram of Pd (=3.15, Table 4) than that shown by the PdZn/Ti-7.5 catalyst, but it should be noted that this sample was measured with a space velocity value half that used with the PdZn/Ti-7.5 catalyst. For this reason, the latter can be considered to have a methanol yield of the same order of magnitude as the most active ones published in the literature. Calculation of apparent activation energy of the most active PdZn/Ti-7.5 catalyst (Fig. 13B) shows its catalyst advantage. It interesting to note that the apparent activation energy for methanol synthesis in PdZn/Ti-7.5 catalyst was 55.5 KJ/mol, that approaches 54 kJ mol^{-1} as measured for conventional CuZnAl catalysts measured under similar reaction conditions, and is lower than the activation energy (68 KJ/mol) reported for other active PdZn intermetallic catalysts also measured under similar reaction conditions [21]. This indicates the effectiveness of the impregnation on TiO_2 with different Zn/Pd ratio using organic precursors used in this work to control the production of PdZn-ZnO interfaces with different activity and selectivity towards methanol.

Finally, the stability of the most active PdZn/Ti-7.5 sample was studied over a longer period of time-on-stream (24 h). As shown in Fig. 13 C, after 8-hour stabilization period, the evolution of methanol yield with time-on-stream was constant and shows no signs of deactivation. This result indicates the stability and absence of deactivation in the PdZn/Ti catalysts and confirms the higher stability of PdZn systems compared to the Cu systems when pure CO_2 is used in the synthesis of methanol.

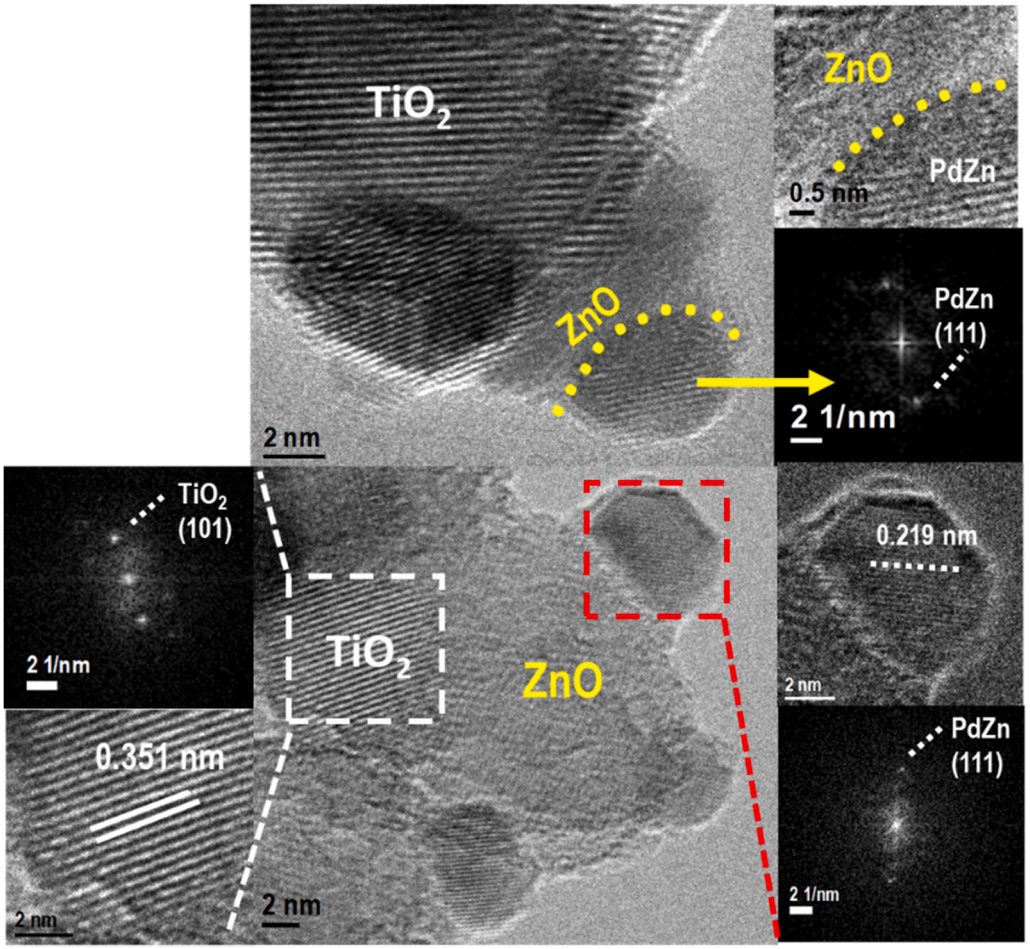

Fig. 10. HRTEM images of reduced PdZn/Ti-5 catalyst and corresponding local FFT and IFFT images of individual PdZn, ZnO and TiO_2 particles.

3.4. Structural (XRD) evolution of used catalysts

The evolution of PdZn and ZnO crystalline phases after reaction was evaluated by comparing the XRD patterns of the freshly reduced and used catalysts (Fig. 14). The used PdZn/Ti catalysts show the same diffraction peaks observed for the freshly reduced catalysts, corresponding to the β-PdZn intermetallic phase, the würtzite-type ZnO hexagonal phase and the anatase phase of the TiO_2 support. The TiO_2 particles do not undergo significant alterations in crystallinity or size after the reaction. However, variations in the intensity of the diffraction peaks of the PdZn and ZnO phases in the samples used with respect to the fresh counterparts are observed as a function of the Zn loading of the catalysts. A slight increase in the intensity of the diffraction peaks of the PdZn phase is observed for the PdZn/Ti-7.5 and especially for the PdZn/Ti-5 samples. The intensity of the diffraction peaks of the ZnO phase also shows a decrease in the used PdZn/Ti-5 and PdZn/Ti-7.5 samples with respect to the reduced samples. The decrease of the intensity of the ZnO diffraction peaks is consistent with the concomitant increase of the intensity of the β-PdZn phase in the used samples, since the formation of PdZn requires the incorporation of reduced Zn atoms [14]. The crystalline domain sizes of TiO_2, ZnO and β-PdZn phases in the catalysts used, determined from the Scherrer equation, are given in Table 5. The crystallite size of intermetallic PdZn in the used catalyst PdZn/Ti-2.5 does not show any significant variation with respect to the freshly reduced sample, while for the used catalysts PdZn/Ti-5 and PdZn/Ti-7.5 there is an increase, particularly in the first case, of the crystallite size of intermetallic PdZn. The absence of PdZn crystallite growth in the case of the PdZn/Ti-2.5 sample could be related to its low ZnO content which does not allow Zn diffusion to form an additional PdZn phase. The formation of additional intermetallic PdZn under reaction conditions, particularly observed for the PdZn/Ti-5 and PdZn/Ti-7.5 catalysts, may be related to the higher hydrogen concentration in the reaction feed, which may facilitate additional ZnO reduction and subsequent intermetallic formation under reaction conditions, as previously reported in the literature [76]. In line with this fact, the higher relative growth of the PdZn phase observed in PdZn/Ti-5 may be related to the smaller particle size of ZnO in this catalyst which may facilitate its reduction under the reaction conditions and the formation of PdZn by migration of reduced Zn. The ZnO phase also shows size variations in the PdZn/Ti catalysts after catalytic tests. In the case of the PdZn/Ti-5 catalyst, a slight decrease in the average size of ZnO crystallites is observed, which is in agreement with the above discussion showing the higher ZnO reduction under the reaction conditions in this sample. In the case of the PdZn/Ti-7.5 catalyst used, the size of ZnO increases slightly under the reaction, with the growth of the polar facet (002), which is in agreement with previous reports showing crystallization of ZnO by water generated during CO_2 hydrogenation [77].

3.5. Catalyst activity-structure correlations

The activity results showed that the impregnation of TiO_2 with different concentrations of ZnO modifies the catalytic behaviour of PdZn/Ti catalysts and, a linear relationship is observed between the increase of Zn concentration in the catalysts and the methanol yield (Fig. 15). The active phase in this reaction is intermetallic PdZn phase. The formation of this intermetallic phase is possible in cases where the metallic Pd is on top of the ZnO nanoparticle and/or right next to it. In this case, TiO_2 acts as a support facilitating the contact between metallic

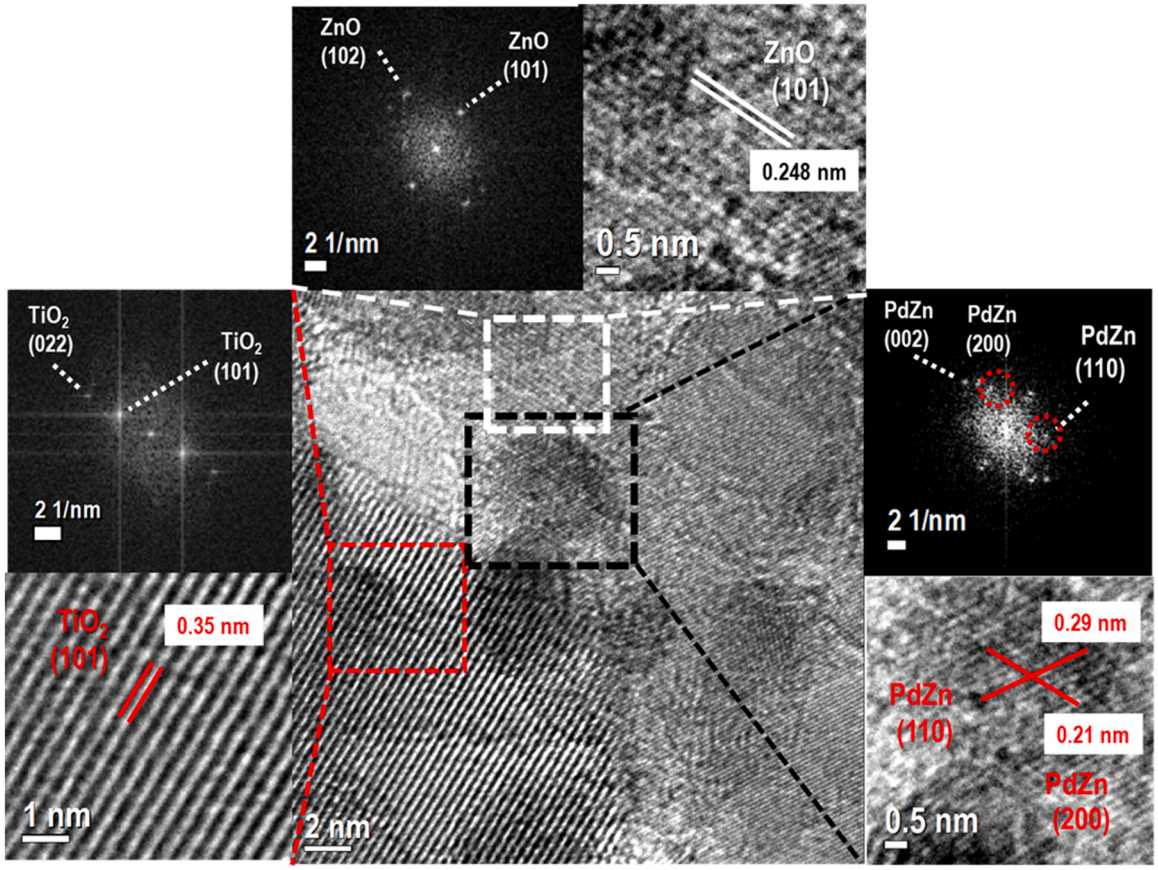

Fig. 11. HRTEM image of reduced PdZn/Ti-7.5 catalyst and corresponding local FFT and IFFT images of individual PdZn, ZnO and TiO_2 particles.

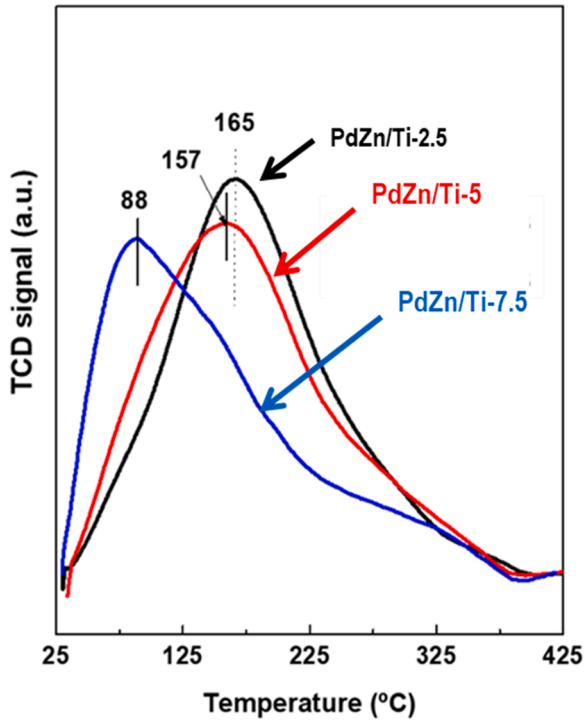

Fig. 12. H_2-TPD profiles of reduced PdZn/Ti catalysts.

Pd and ZnO. The physicochemical characterization of calcined PdZn/Ti catalysts by XRD and H_2-TPR has shown that, in general, increasing the Zn concentration in the catalysts leads to a slight increase in the dispersion of the PdO particles and an increase in the crystallinity and size of the ZnO particles. These characteristics of the calcined catalysts govern the formation of PdZn species and their interaction with ZnO after the reduction process. At this point, it should be noted that the use of organic Pd and Zn precursors in the impregnation of TiO_2 has made it possible to achieve the formation of PdO and ZnO nanoparticles that facilitate the uniform formation of intermetallic PdZn particles, since it is known that the diffusion of Zn atoms in small Pd particles is easier than in the case of large particles that can lead to the formation of elemental Pd or Zn-poor intermetallic compounds [43]. The presence of small intermetallic β-PdZn particles was confirmed for all PdZn/Ti catalysts by XRD and HRTEM with no significant differences in formation temperature, crystallinity or size of intermetallic PdZn particles observed when varying the Zn concentration in the catalysts. In fact, the reduction onset temperature for PdZn particle formation was observed at a similar temperature (250 °C, Fig. 6B) and intermetallic PdZn particles of similar crystallinity and size (4–6 nm, Fig. 8, Table 5) were obtained for all PdZn/Ti catalysts regardless of Zn concentration. However, the differences were in the characteristics of the ZnO particles, which varied in the reduced PdZn/Ti catalysts with varying Zn concentration. The ZnO particles in the reduced catalysts increase in size and crystallinity with increasing Zn concentration, as deduced from XRD (Fig. 14A) and HRTEM data (Figs. 9–11). The differences in ZnO particle characteristics lead to remarkable changes in the development of the contacts of the ZnO particles with the PdZn intermetallic compounds in the reduced PdZn/Ti catalysts as demonstrated by TEM and CO-DRIFTS data. This is probably associated with the increased probability of establishing PdZn-ZnO_x contacts with increasing ZnO loading, but also

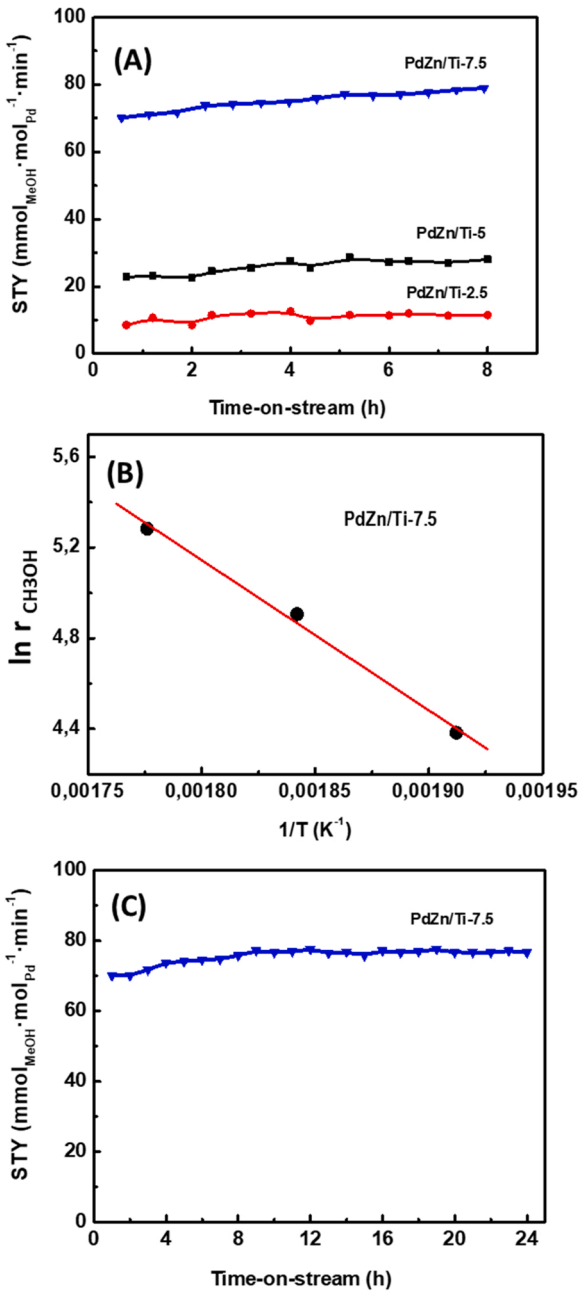

Fig. 13. (A) Comparison of methanol yield from CO_2 for PdZn/Ti-2.5, PdZn/Ti-5 and PdZn/Ti-7.5 catalysts. (B Arrhenius plot for methanol synthesis over PdZn/Ti-7.5 catalyst. (C) Evolution of methanol yield in the stability test (24 h) over PdZn/Ti-7.5 catalyst (T = 250 °C; P = 30 bar; CO_2/H_2 ratio =1:3, GHSV=12,000 mL(N)($CO_2/H_{2\ feed}$) gcat^{-1}h^{-1}).

with the different development of the ZnO crystal structures in the catalysts because, as postulated in the literature [49,78], the efficiency of the formation of stable β-PdZn/ZnO interfaces is higher in the polar (002) planes of ZnO, whose relative concentration in PdZn/Ti catalysts increases with increasing Zn concentration, as shown by XRD (Fig. 14A).

In the work presented here, catalysts with a similar development of intermetallic β-PdZn particles show a dependence of methanol production on Zn concentration (Fig. 15). These results contrast with the recent work of Bowker et al. [18], which showed that the activity of Pd/ZnO catalysts was mainly determined by the presence of the intermetallic β-PdZn compound. A possible reason for this discrepancy may be related to the fact that in the cited work, the catalysts are PdZn-ZnO systems supported on ZnO, in which there is a large excess of Zn with respect to

Table 3
Activity data in methanol synthesis from CO_2 on reduced PdZn/Ti catalysts and Pd/TiO_2 (as reference) (T = 250 °C; P = 30 bar; CO_2:H_2 = 1:3 mol:mol; 50 mL (N)min^{-1}; TOS= 8 h).

	CO_2 conv. (%)	Select. CH_3OH (%)	Select. CO (%)	Select. CH_4 (%)	CH_3OH yield ($mmol_{MeOH}$ min^{-1} mol_{Pd}^{-1})
Pd/TiO_2	5.9	0	96.0	4.0	0
PdZn/Ti-2.5	0.55	48.8	51.2	0.0	13.1
PdZn/Ti-5	0.86	64.6	35.4	0.0	30.3
PdZn/Ti-7.5	2.55	58.2	41.8	0.0	78.9

Table 4
Comparison of CO_2 conversion, CH_3OH selectivity and yield on the PdZn/Ti-7.5 catalyst with other PdZn-based catalysts reported in the literature for methanol synthesis from CO_2 hydrogenation under same temperature and pressure (T = 250 °C, P = 30 bar).

	Pd (wt %)	GSHV (mL g^{-1}·h^{-1})	CO_2 conv. (%)	CH_3OH select. (%)	CH_3OH Yield (g·g_{Pd}^{-1}·h^{-1})	Ref.
PdZn/Ti-7.5	3.8	12,000	2.55	58.2	1.44	This work
Pd/ZnO	2.5	6000	5.8	68.9	3.15	[30]
PdZnAl	1.5	13,440	0.6	60	1.37	[21]
PdZn/CNTs	16	1800	6.3	99,6	0,23	[77]
PdZn-Al_2O_3	20	1800	4.4	96.5	0.12	[77]

Pd. This contrasts with the PdZn-ZnO systems supported on TiO_2 studied in this work with much higher Pd/Zn ratio and for which the effects of Zn concentration are more significant. However, our results are consistent with the work of Bokhoven et al. [19] with PdZn-ZnO supported systems that have shown that the PdZn intermetallic phase by itself is not particularly active for the direct hydrogenation of CO_2 to methanol, and only when ZnO and PdZn intermetallic particles are present, the activity and selectivity to methanol increases because the selective hydrogenation of CO_2 to methanol takes place predominantly at the interface of the ZnO with the PdZn intermetallic particles. Although the mechanism of methanol synthesis from CO_2 on PdZn-ZnO is not fully explained [30], the main hypothesis to explain the role of the contacts between PdZn and ZnO in the synthesis of methanol from CO_2 is based in a bifunctional mechanism where the contacts between PdZn and ZnO stabilise the intermediate species formed from CO_2 activation on ZnO surfaces and hydrogen dissociation on the intermetallic PdZn particles. The nature of the intermediate species is still under discussion and some works point to formate species (considering that PdZn/ZnO behaves similarly to the widely studied Cu/ZnO systems [14,19]) while others point to carbonate species (based on in-situ DRIFTS studies [30]). These intermediates are hydrogenated to methanol by hydrogen atoms at the PdZn-ZnO interface, as visualized in Fig. 16. In fact, the TPR and H_2-TPD results suggest that increasing the ZnO content in the PdZn/Ti catalysts enhances the hydrogen spillover from the intermetallic PdZn to ZnO. Under this hypothesis, the enhancement of catalyst activity observed with increasing Zn concentration is associated to an increase of PdZn-ZnO interfacial sites where, therefore, CO_2 adsorption and hydrogenation of intermediate species to methanol increases [79].

Changes in methanol selectivity were observed among the PdZn/Ti catalysts (Table 3). The low methanol selectivity achieved on the PdZn/Ti-2.5 catalyst could be related to the poor development of PdZn-ZnO contacts in this sample since, as discussed above, in the absence of these contacts, the PdZn phase has little activity and selectivity for methanol production. In the case of PdZn/Ti-5 and PdZn/Ti-7.5, the

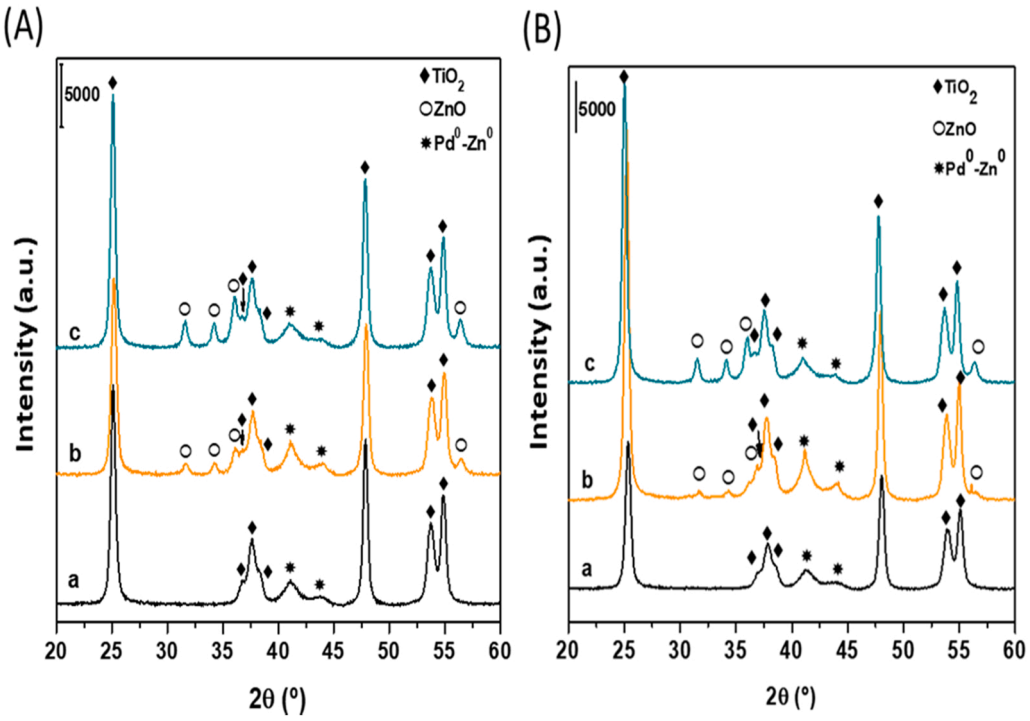

Fig. 14. X-ray diffraction patterns of the fresh reduced PdZn/Ti catalysts (A) and used catalysts (B): PdZn/Ti-2.5 (a); PdZn/Ti-5 (b), and PdZn/Ti-7.5 (c).

Table 5
Mean crystallite size (XRD) for reduced and used PdZn/Ti catalysts.

	Crystallite size (nm)					
	TiO_2		ZnO		PdZn (111)	
	Reduced	used	reduced	used	reduced	used
PdZn/Ti-2.5	16.2	15.0	n.d.	n.d.	5.3	5.1
PdZn/Ti-5	15.3	17.8	11.6 (100) 12.8 (002)	9.6 (100) 8.6 (002)	6.2	8.2
PdZn/Ti-7.5	16.9	17.7	13.8 (100) 13.7 (002) 12.0 (101)	14.1 (100) 14.0 (002) 11.9 (101)	4.6	5.6

n.d.: non-detected

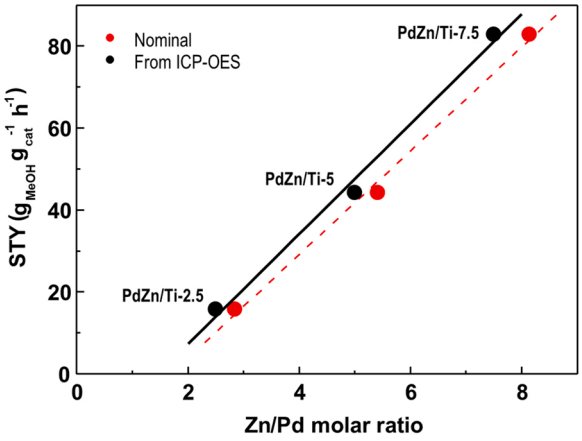

Fig. 15. Effect of Zn/Pd molar ratio on the efficiency of PdZn/Ti catalysts towards methanol production.

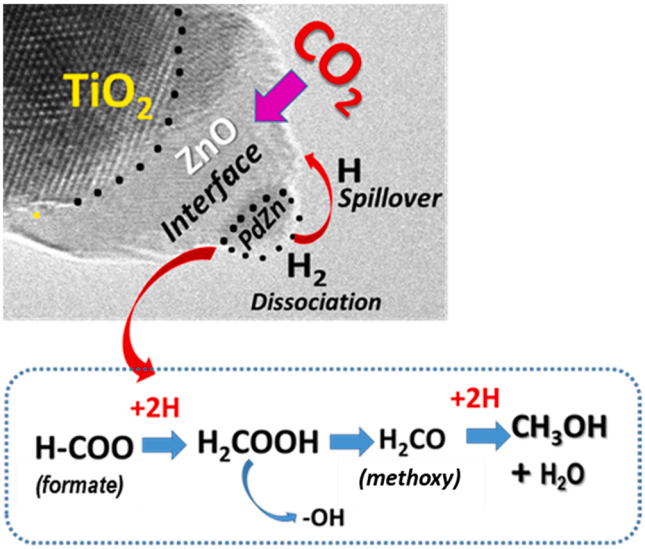

Fig. 16. Scheme visualizing the adsorption of CO_2 at the PdZn-ZnO interface and the hydrogen dissociation on the intermetallic PdZn surface followed by its spillover of the formed atomic hydrogen to hydrogenate the reaction intermediates.

decrease in selectivity towards methanol formation with increasing CO_2 conversion is in line with the observed linear relationship between selectivity and conversion for PdZn materials [18]. However, we observed another interesting factor that could affect the observed decrease in methanol selectivity, namely the strong differences in the crystallinity and size of ZnO phase in the PdZn/Ti-5 and PdZn/Ti-7.5 catalysts that affect their stability under reaction conditions. In this regard, the smaller and less crystalline ZnO particles of PdZn/Ti-5 are unstable under reaction conditions, undergoing greater reduction and transformation than the ZnO particles of the PdZn/Ti-7.5 catalyst (Fig. 13 B), which, due to their larger size and crystallinity, offer greater

stability after reaction. This is an important finding of this work that could explain many results reported in the literature for CO_2 hydrogenation to methanol over PdZn-based catalysts. In this regard, new work is being carried out in our laboratory on PdZn intermetallic compounds in contact with ZnO particles supported on different substrates.

4. Conclusions

The use of organic Pd and Zn precursors in the impregnation of TiO_2 has made it possible to achieve the formation of PdO and ZnO nanoparticles that facilitate the formation of small intermetallic β-PdZn particles. The presence of small intermetallic β-PdZn particles was confirmed for all catalysts with no significant differences in formation, crystallinity or size of intermetallic particles when varying the Zn concentration in the supported catalysts. The differences were in the characteristics of ZnO particles that lead to remarkable changes in the development of the contacts of ZnO particles with the PdZn intermetallic compounds in reduced PdZn/Ti catalysts. Enhanced development of the contacts between the PdZn and ZnO particles was observed as the Zn loading on the catalysts increases. This is associated with the increase in the efficiency for the formation of stable β-PdZn/ZnO interfaces in the polar planes of ZnO, whose relative concentration in PdZn/Ti catalysts increases with increasing Zn concentration. In the work presented here, catalysts with a similar development of intermetallic β-PdZn particles show a linear relationship between the increase of Zn concentration in the catalysts and the methanol yield showing the important role of ZnO loading in the catalytic activity. The activity to methanol increases because the selective hydrogenation of CO_2 to methanol takes place predominantly at the interface of the ZnO with the PdZn intermetallic particles that increases in the PdZn/Ti catalysts as the Zn loading increases. The differences in the crystallinity and size of the ZnO phase in the PdZn/Ti catalysts also affect their stability under the reaction conditions. The smaller and less crystalline ZnO particles are unstable under the reaction conditions, undergoing greater reduction and transformation than the larger ZnO particles which offer greater stability under the reaction conditions. The methanol yield over the catalyst with the highest Zn loading (PdZn/Ti-7.5) reaches 1.44 g of $CH_3OH/(g_{Pd}\ h)$, which is in line with the highest values of the supported PdZn catalysts reported in the literature under similar reaction conditions. This indicates the effectiveness of the impregnation on TiO_2 with different Zn/Pd ratio using organic precursors used in this work to control the production of PdZn-ZnO interfaces with different activity and selectivity towards methanol.

CRediT authorship contribution statement

Carlos Quilis: (Investigation, Review) and **Noelia Mota:** (Investigation, Draft preparation, Research); **Barbara Pawelec:** (Methodology, writing); **Elena Millán:** (Investigation); **Rufino M. Navarro:** (Conceptualization, Methodology, Supervision and Writing). All authors have read and accepted the published version of the manuscript.

Funding

The present investigation was performed within the research program PID2019-111219RB-100 supported by the Spanish Ministry of Science, Innovation and Universities. The Autonomus Community of Madrid (CAM) is also gratefully acknowledged for funding BIOTRES-CM (P2018/EMT-4344) project. Elena Millán and Carlos Quilis would like to acknowledge the FPI programme from Spanish Ministry of Science, Innovation and Universities for their research grants.

Declaration of Competing Interest

The authors declare that they have no known competing financial interests or personal relationships that could have appeared to influence the work reported in this paper.

Data Availability

Data will be made available on request.

References

[1] U. Etim, Y. Song, Z. Zhonh, Improving the Cu/ZnO-based catalysts for carbon dioxide hydrogenation to methanol, and the use of methanol as a renewable energy storage media, Front. Energy Res. 8 (2020), 545431.
[2] G.A. Olah, Beyond oil and gas: the methanol economy, Angew. Chem. Int. Ed. 44 (2005) 2636–2639.
[3] O.A. Ojelade, S.F. Zaman, A review on Pd based catalysts for CO_2 hydrogenation to methanol: in-depth activity and DRIFTS mechanistic study, Catal. Surv. Asia 24 (2020) 11–37.
[4] R. Guil-López, N. Mota, J. Llorente, E. Millán, B. Pawelec, J.L.G. Fierro, R. M. Navarro, Methanol synthesis from CO_2: a review of the latest developments in heterogeneous catalysis, Materials 12 (2019), 3902.
[5] M. Gentzen, D.E. Doronkin, T.L. Sheppard, A. Zimina, H. Li, J. Jelic, F. Studt, J.-D. Grunwaldt, J. Sauer, S. Behrens, Supported intermetallic PdZn nanoparticles as bifunctional catalysts for the direct synthesis of dimethyl ether from CO-rich synthesis gas, Angew. Chem. Int. Ed. 58 (2019) 15655–15659.
[6] Y. Matsumura, Stabilization of $Cu/ZnO/ZrO_2$ catalyst for methanol steam reforming to hydrogen by coprecipitation on zirconia support, J. Power Sources 238 (2013) 109–116.
[7] T. Witoon, J. Chalorngtham, P. Dumrongbunditkul, M. Chareonpanich, J. Limtrakul, CO_2 hydrogenation to methanol over Cu/ZrO_2 catalysts: Effects of zirconia phases, Chem. Eng. J. 293 (2016) 327–336.
[8] S. Kattel, P.J. Ramírez, J.G. Chen, J.A. Rodriguez, P. Liu, Active sites for CO_2 hydrogenation to methanol on Cu/ZnO catalysts, Science 355 (2017) 1296–1299.
[9] S. Kuld, Quantifying the promotion of Cu catalysts by ZnO for methanol synthesis, Science 352 (2016) 969–974.
[10] A. Vourros, I. Garagounis, V. Kyriakou, S.A. Carabineiro, F.J. Maldonado-Hódar, G. E. Marnellos, M. Konsolakis, Carbon hydrogenation over supported Au nanoparticles: effect of the support, J. CO_2 Util. 19 (2017) 247–256.
[11] R. Grabowski, J. Sloczynski, M. Sliwa, D. Mucha, R.P. Socha, Influence of polymorphic ZrO_2 phases and the silver electronic state on the activity of Ag/ZrO_2 catalysts in the hydrogenation of CO_2 to methanol, ACS Catal. 1 (2011) 266–278.
[12] O. Martin, A.J. Martín, C. Mondelli, S. Mitchell, T.F. Segawa, R. Hauert, C. Drouilly, D. Curulla-Ferre, J. Perez-Ramirez, Indium oxide as a superior catalyst for methanol synthesis by CO_2 hydrogenation, Angew. Chem. Int. Ed. 55 (2016) 6261–6265.
[13] J. Xu, X. Su, X. Liu, X. Pan, G. Pei, Y. Huang, X. Wang, T. Zhang, H. Geng, Methanol synthesis from CO_2 and H_2 over $PdZn/ZnO/Al_2O_3$: Catalyst structure dependence of methanol selectivity, Appl. Catal. A Gen. 514 (2016) 51–59.
[14] H. Bahruji, M. Bowker, G. Hutchings, N. Dimitratos, P. Wells, E. Gibson, W. Jones, C. Brookes, D. Morgan, G. Lalev, PdZn/ZnO catalysts for direct CO_2 hydrogenation to methanol, J. Catal. 343 (2016) 133–146.
[15] N. Iwasa, H. Suzuki, M. Terashita, M. Arai, N. Takezawa, Methanol synthesis from CO_2 under atmospheric pressure over supported Pd catalysts, Catal. Lett. 96 (2004) 75–78.
[16] A.S. Malik, S.F. Zaman, A.A. Al-Zahrani, M.A. Daous, H. Driss, L.A. Petrov, Selective hydrogenation of CO_2 to CH_3OH and in-depth DRIFT analysis for $PdZn/ZrO_2$ and $CaPdZn/ZrO_2$ catalysts, Catal. Today 357 (2020) 573–582.
[17] X.-L. Liang, X. Dong, G.-D. Lin, H.-B. Zhang, Carbon nanotube-supported Pd-ZnO catalyst for hydrogenation of CO_2 to methanol, Appl. Catal. B Environ. 88 (2009) 315–322.
[18] M. Bowker, N. Lawes, I. Gow, J. Hayward, J. Ruiz Esquius, N. Richards, L.R. Smith, T.J.A. Slater, T.E. Davies, N.F. Dummer, L. Kabalan, A. Logsdail, R.C. Catlow, S. Taylor, G.J. Hutchings, The critical role of β-PdZn alloy in PdZn/ZnO catalysts for the hydrogenation of carbon dioxide to methanol, ACS Catal. 12 (2022) 5371–5379.
[19] M. Zabilskiy, V.L. Sushkevich, M.A. Newton, F. Krumeich, M. Nachtegaal, J.A. van Bokhoven, Mechanistic study of carbon dioxide hydrogenation over PdZn/ZnO-based catalysts: The role of Palladium–Zinc alloy in selective methanol synthesis, Angew. Chem. Int. Ed. 60 (2021) 17053–17059.
[20] H. Bahruji, J.R. Esquius, M. Bowker, G. Hutchings, R.D. Armstrong, W. Jones, Solvent free synthesis of $PdZn/TiO_2$ catalysts for the hydrogenation of CO_2 to methanol, Top. Catal. 61 (2018) 144–153.
[21] A. Ota, E.L. Kunkes, I. Kasatkin, E. Groppo, D. Ferri, B. Poceiro, R.M.N. Yerga, M. Behrens, Comparative study of hydrotalcite-derived supported Pd_2Ga and PdZn intermetallic nanoparticles as methanol synthesis and methanol steam reforming catalysts, J. Catal. 293 (2012) 27–38.
[22] V.M. Lebarbier, R.A. Dagle, L. Kovarik, J.A. Lizarazo-Adarme, D.L. King, D.R. Palo, Synthesis of methanol and dimethyl ether over $Pd/ZnO/Al_2O_3$ catalysts, Catal. Sci. Technol. 2 (2012) 2116–2127.
[23] F. Liao, X.-P. Wu, J. Zheng, M. Li, A. Kroner, Z. Zeng, X. Hong, Y. Yuan, X.-G. Gong, S.C.E. Tsang, A promising low pressure methanol synthesis route from CO_2 hydrogenation over Pd@Zn core–shell catalysts, Green Chem. 19 (2017) 270–280.
[24] Y. Wang, D. Wu, T. Liu, G. Liu, X. Hong, Fabrication of PdZn alloy catalysts supported on ZnFe composite oxide for CO_2 hydrogenation to methanol, J. Colloid Interface Sci. 597 (2021) 260–268.

[25] F. Liao, X.-P. Wu, J. Zheng, M. Li, A. Dent, Z. Zeng, X. Hong, A. Kroner, Y. Yuan, X.-G. Gong, S.C.E. Tsang, Pd@Zn core-shell nanoparticles of controllable shell thickness for catalytic methanol production, Catal. Sci. Technol. 6 (2016) 7698–7702.

[26] J. Riuz Esquius, H. Bahruji, S.H. Taylor, M. Bowker, G.J. Hutchings, CO_2 hydrogenation to methanol over PdZn catalysts with reduced methane production, ChemCatChem 12 (2020) 6024–6032.

[27] H. Bahruji, M. Bowker, W. Jones, J. Hayward, J. Ruiz Esquius, D.J. Morgan, G. J. Hutchings, PdZn catalysts for CO_2 hydrogenation to methanol using chemical vapour impregnation (CVI), Faraday Discuss. 197 (2017) 309.

[28] J. Zhong, X. Yang, Z. Wu, B. Liang, Y. Huang, T. Zhang, State of the art and perspectives in heterogeneous catalysis of CO_2 hydrogenation to methanol, Chem. Soc. Rev. 49 (2020) 1385.

[29] O.A. Ojelade, S.F. Zaman, M.A. Daous, A.A. Al-Zahrani, A.S. Malik, H. Driss, G. Shterk, J. Gascon, Optimizing Pd:Zn molar ratio in PdZn/CeO_2 for CO_2 hydrogenation to methanol, Appl. Catal. A Gen. 584 (2019), 117185.

[30] J. Song, S. Liu, C. Yang, G. Wang, H. Tian, Z.-J. Zhao, R. Mu, J. Gong, The role of Al doping in Pd/ZnO catalyst for CO_2 hydrogenation to methanol, Appl. Catal. B 263 (2020) 18367.

[31] Y. Yin, B. Hu, X. Li, X. Zhou, X. Hong, G. Liu, Pd@zeolitic imidazolate framework-8 derived PdZn alloy catalysts for efficient hydrogenation of CO_2 to methanol, Appl. Catal. B 234 (2018) 306–311.

[32] F. Brix, V. Desbuis, L. Piccolo, É. Gaudry, Tuning adsorption energies and reaction pathways by alloying: PdZn versus Pd for CO_2 hydrogenation to methanol, J. Phys. Chem. Lett. 11 (2020) 7672–7678.

[33] E. Nowicka, S.M. Althaban, Y. Luo, R. Kriegel, G. Shaw, D.J. Morgan, Q. He, M. Watanabe, M. Ambrüster, C.J. Kiely, G. Hutchings, Highly selective PdZn/ZnO catalysts for the methanol stream reforming reaction, Catal. Sci. Technol. 8 (2018) 5848–5857.

[34] N. Iwasa, T. Mayanagi, S. Masuda, N. Takezawa, Steam reforming of methanol over PdZn catalysts, React. Kinet. Catal. Lett. 69 (2000) 355.

[35] N. Iwasa, T. Mayanagi, W. Nomura, M. Arai, N. Takezawa, Effect of Zn addition to supported Pd catalysts in the steam reforming of methanol, Appl. Catal. A: Gen. 248 (2003) 153–160.

[36] N. Iwasa, N. Takezawa, New supported Pd and Pt alloy catalysts for steam reforming and dehydrogenation of methanol, Top. Catal. 22 (2003) 215.

[37] M. Armbrüster, M. Behrens, K. Föttinger, M. Friedrich, É. Gaudry, S. Matam, H. Sharma, The intermetallic compound ZnPd and its role in methanol steam reforming, Catal. Rev. 55 (2013) 289–367.

[38] P. Yan, P. Tian, C. Cai, S. Zhou, X. Yu, S. Zhao, X. Yu, S. Zhao, S.-T. Tu, C. Deng, Y. Sun, Antioxidative and stable PdZn/ZnO/Al_2O_3 catalyst coatings concerning methanol steam reforming for fuel cell-powered vehicles, Appl. Energy 268 (2020), 115043.

[39] Y.-H. Chin, R. Dagle, J. Hu, A.C. Dohnalkova, Y. Wang, Steam reforming of methanol over highly active Pd/ZnO catalyst, Catal. Today 77 (2002) 79–88.

[40] P. Kast, M. Friedrich, F. Girgsdies, J. Kröhnert, D. Teschner, T. Lunkenbein, M. Behrens, R. Schlögl, Strong metal-support interaction and alloying in PdZn/ZnO catalysts for CO oxidation, Catal. Today 260 (2016) 21–31.

[41] R.S. Johnson, A. De La Riva, V. Ashbacher, B. Halevi, C.J. Villanueva, G.K. Smith, S. Lin, A.K. Datye, H. Guo, The CO oxidation mechanism and reactivity on PdZn alloys, Phys. Chem. Chem. Phys. 15 (2013) 7768–7776.

[42] E. Nowicka, S. Althahban, T.D. Leah, G. Shaw, D. Morgan, C.J. Kiely, G. J. Hutchings, Benzyl alcohol oxidation with Pd-Zn/TiO_2: computational and experimental studies, Sci. Technol. Adv. Mater. 20 (1) (2019) 367–378.

[43] E. Castillejos-López, G. Agostini, M. Di Michel, A. Iglesias-Juez, B. Bachiller-Baeza, Synergy of contact between ZnO surface planes and PdZn nanostructures: morphology and chemical property effects in the intermetallic sites for selective 1,3-butadiene hydrogenation, ACS Catal. 7 (2017) 796–811.

[44] C. Liu, Y. Shi, Y. Shang, X. Wang, D. Liu, B.B. Mamba, A.T. Kuvarega, J. Gui, Promoting effect of PdZn alloy for selective hydrogenation of 5-hydroxylmethyl-furfural: an experimental and density functional theory study, Int. J. Quantum Chem. 121 (6) (2021), e26545.

[45] P.L. Berlowitz, D.W. Goodman, The activity of Pd(110) for methanol synthesis, J. Catal. 108 (1987) 364–368.

[46] D.V. Glyzdova, E.V. Khramov, N.S. Smirnovac, I.P. Prosvirind, A.V. Bukhtiyarovd, M.V. Trenikhina, T.I. Gulyaevaa, A.A. Vedyagind, D.A. Shlyapina, A.V. Lavrenova, Study on the active phase formation of Pd-Zn/Sibunit catalysts during the thermal treatment in hydrogen, Appl. Surf. Sci. 483 (2019) 730–741.

[47] J. De Waele, V.V. Galvita, H. Poelman, C. Detavernier, J.W. Thybaut, Formation and stability of an active PdZn nanoparticle catalyst on a hydrotalcite-based support for ethanol dehydrogenation, Catal. Sci. Technol. 7 (2017) 3715.

[48] C.-H. Kim, J.S. Lee, D.L. Trimm, The preparation and characterization of Pd-ZnO catalysts for methanol synthesis, Top. Catal. 22 (2003) 319–324.

[49] H. Zhang, J. Sun, V.L. Dagle, B. Halevi, A.K. Datye, Y. Wang, Influence of ZnO facets on Pd/ZnO catalysts for methanol steam reforming, ACS Catal. 4 (2014) 2379–2386.

[50] E.P. Barrett, L.G. Joyner, P.H. Halenda, The determination of pore volume and area distributions in porous substances. I. Computations from nitrogen isotherms, J. Am. Chem. Soc. 73 (1951) 373–380.

[51] R. Obeso-Estrella, B. Pawelec, N. Mota, L. Flores, J.M.O. Melgoza, R.I. Yocupicio-Gaxiola, T.A. Zepeda, Elucidating the mechanisms of titanium–induced morphological and structural changes in catalysts on mesoporous Al_2O_3–TiO_x mixed oxides: effect of non–stoichiometric TiO_x phase, Microporous Mesoporous Mater. 339 (2022) article 111991.

[52] J. Cai, Z. Huang, K. Lv, J. Sun, K. Deng, Ti powder-assisted synthesis of Ti^{3+} self-doped TiO_2 nanosheets with enhanced visible light photoactivity, RSC Adv. 4 (2014) 19588–19593.

[53] K.A. Alim, V.A. Fonoberov, M. Shamsa, A.A. Balandin, Micro-Raman investigation of optical phonons in ZnO nanocrystals, J. Appl. Phys. 97 (2005) 124313–124314.

[54] J. Chen, Z. Feng, P. Ying, C. Li, ZnO clusters encapsulated inside micropores of zeolites studied by UV Raman and laser-induced luminescence spectroscopies, J. Phys. Chem. B 108 (2004) 12669–12676.

[55] K.S.W. Sing, D.H. Everett, R.A.W. Haul, L. Moscou, R.A. Pierotti, J. Rouquérol, T. Siemieniewska, Reporting physisorption data for gas/solid systems with special reference to the determination of surface area and porosity (recommendations 1984), Pure Appl. Chem. 57 (1985) 603–619.

[56] C. Amorim, M.A. Keane, Palladium supported on structured and nonstructured carbon: a consideration of Pd particle size and the nature of reactive hydrogen, J. Colloid Interface Sci. 322 (2008) 196–208.

[57] R.M. Navarro, B. Pawelec, J.M. Trejo, R. Mariscal, J.L.G. Fierro, Hydrogenation of aromatics on sulfur-resistant PtPd bimetallic catalysts, J. Catal. 189 (2000) 184–194.

[58] M. Nag, A study on the formation of palladium hydride in a carbon-supported palladium catalyst, J. Phys. Chem. B 105 (2001) 5945–5949.

[59] C.T. Hong, C.-T. Yeh, F.H. Yu, Effect of reduction and oxidation treatments on PdZn/ZnO catalysts, Appl. Catal. 48 (1989) 385–396.

[60] Y. Niu, Y. Xi, Y. Wang, S. Zhou, Z. Lv, L. Zhang, W. Shi, Y. Li, W. Zhang, Su.S. Dang, B. Zhang, Formation of intermetallic PdZn in a palladium/zinc oxide catalyst: interfacial fertilization by PdH, Angew. Chem. Int. Ed. 58 (13) (2019) 4232–4237.

[61] S. Penner, B. Jenewein, H. Gabasch, B. Kloetzer, D. Wang, A. Knop-Gericke, R. Schloegl, K. Hayek, Growth and structure stability of well-ordered PdZn alloy nanoparticles, J. Catal. 241 (2006) 14–19.

[62] A. Ashrafi, C. Jagadish, Review of zinc blende ZnO: stability of metastable ZnO phases, J. Appl. Phys. 102 (2007), 071101.

[63] A. Kołodziejczak-Radzimska, T. Jesionowski, Zinc oxide - from synthesis to application: a review, Materials 7 (2014) 2833–2881.

[64] N. Muñoz-Aguirre, L. Martínez-Pérez, S. Muñoz-Aguirre, L.A. Flores-Herrera, E. Vergara Hernández, O. Zelaya-Angel, Luminescent properties of (004) highly oriented cubic zinc blende ZnO thin films, Materials 12 (2019) 3314.

[65] S.-K. Kim, S.-Y. Jeong, C.-R. Cho, Structural reconstruction of hexagonal to cubic ZnO films on Pt/Ti/SiO_2/Si substrate by annealing, Appl. Phys. Lett. 82 (2003) 562.

[66] T. Lear, R. Marshall, J.A. Lopez-Sanchez, S.D. Jackson, T.M. Klapötke, M. Bäumer, G. Rupprechter, H.J. Freund, D. Lennon, The application of infrared spectroscopy to probe the surface morphology of alumina-supported palladium catalysts, J. Chem. Phys. 123 (2005), 174706.

[67] P. Ruzzi, D. Salusso, M. Baravaglio, K.C. Szeto, A. De Mallmann, L. Gil Jiménez, C. Godard, A. Benayad, S. Morandi, S. Bordiga, M. Taoufik, Supported PdZn nanoparticles for selective CO_2 conversion, through the grafting of a heterobimetallic complex on $CeZrO_x$, Appl. Catal. A Gen. 635 (2022), 118568.

[68] I.D. González, R.M. Navarro, M.C. Álvarez-Galván, F. Rosa, J.L.G. Fierro, Performance enhancement in the water-gas shift reaction of platinum deposited over a cerium-modified TiO_2 support, Catal. Comm. 9 (8) (2008) 1759–1765.

[69] A. Bonilla Sánchez, N. Homs, S. Miachon, J. Dalmon, J.L.G. Fierro, P. Ramírez De La Piscina, Direct transformation of ethanol into ethyl acetate through catalytic membranes containing Pd or Pd-Zn: comparison with conventional supported catalysts, Green Chem. 13 (2011) 2569–2575.

[70] J. Araña, N. Homs, J. Sales, J.L.G. Fierro, P. Ramírez de la Piscina, CO/CO_2 hydrogenation and ethylene hydroformylation over silica-supported PdZn catalysts, Catal. Lett. 72 (2001) 183–189.

[71] D.J. Childers, N.M. Schweitzer, S.M. Kamali Shahari, R.M. Rioux, J.T. Miller, R. J. Meyer, Modifing structure-sensitive reactions by addition of Zn to Pd, J. Catal. 318 (2014) 75–84.

[72] K. Föttinger, The effect of CO on intermetallic PdZn/ZnO and Pd_2Ga/Ga_2O_3 methanol steam reforming catalysts: a comparative study, Catal. Today 208 (2013) 106–112.

[73] P. Kast, M. Friedrich, F. Girgsdies, J. Kröhnert, D. Teschner, T. Lunkenbein, M. Behrens, R. Schlögl, Strong metal-support interaction and alloying in Pd/ZnO catalysts for CO oxidation, Catal. Today 260 (2016) 21–31.

[74] W. Yanhua, Z. Jingchang, X. Hengyong, Interaction between Pd and ZnO during reduction of Pd/ZnO catalyst for steam reforming of methanol to hydrogen, Chin. J. Catal. 27 (2006) 217–222.

[75] X.L. Liang, X. Dong, G.D. Lin, H. Bin Zhang, Carbon nanotube-supported Pd-ZnO catalyst for hydrogenation of CO_2 to methanol, Appl. Catal. B Environ. 88 (3–4) (2009) 315–322.

[76] N. Iwasa, T. Akazawa, S. Ohyama, K. Fujikawa, N. Takezawa, React. Kinet. Catal. Lett. 55 (1995) 245–250.

[77] J. Wu, M. Saito, M. Takeuchi, T. Watanabe, The stability of Cu/ZnO-based catalysts in methanol synthesis from a CO_2-rich feed and from a CO-rich feed, Appl. Catal., A 218 (2001) 235–240.

[78] M.P. Hyman, V.M. Lebarbier, Y. Wang, A.K. Datye, J.M. Vohs, A comparison of the reactivity of Pd supported on ZnO($10\bar{1}0$) and ZnO(0001), J. Phys. Chem. C. 113 (2009) 7251–7259.

[79] N. Rui, Z. Wang, K. Sun, J. Ye, Q. Ge, C.-J. Liu, CO_2 hydrogenation to methanol over Pd/In_2O_3: effects of Pd and oxygen vacancy, Appl. Catal. B Environ. 218 (2017) 488–497.